



Sarah Rendl, BSc

Time-Dependent Water Uptake in Polymer-Based Nanocomposites

MASTERARBEIT

Zur Erlangung des akademischen Grades

Diplom-Ingenieurin

Masterprogramm Technische Chemie

Eingereicht an der

Technischen Universität Graz

Betreuer

Priv.-Doz. Dipl.-Chem.Univ. Dr.rer.nat. Frank Wiesbrock

Institute for Chemistry and Technology of Materials

Graz, Dezember 2018

Eidesstattliche Erklärung / Statutory Declaration

I declare that I have authored this thesis independently, that I have not used other than the declared sources / resources, and that I have explicitly marked all material which has been quoted either literally or by content from the used sources.

Date

Signature

Ich erkläre, dass ich diese Arbeit unabhängig verfasst habe, dass ich keine anderen als die angegebenen Quellen / Ressourcen verwendet habe und dass ich ausdrücklich jedes Material markiert habe, das entweder aus den verwendeten Quellen wörtlich oder nach Inhalten zitiert wurde.

Datum

Unterschrift

Acknowledgement

The research work of this master thesis was performed within the K-Project 'PolyTherm' at the Polymer Competence Center Leoben GmbH (PCCL) within the framework of the COMET-program of the Federal Ministry for Transport, Innovation and Technology and the Federal Ministry of Digital and Economic Affairs with contributions by the Graz University of Technology and the Montanuniversitaet Leoben.

First, I would like to thank Priv.-Doz. Dipl.Chem.Univ. Dr.rer.nat. Frank Wiesbrock for his benevolent support, technical assistance and the scientific discussions during this work.

Secondly, I am indebted to Michael Feuchter, Helena Weingrill, and Andrea Anusic for the help and advice he gave me on the performance of the differential scanning calorimetry measurements. Furthermore, I owe thanks to Karin Wewerka for the detailed investigations with the transmission electron microscopy. Moreover, I would like to thank Petra Kaschnitz for her support concerning the NMR measurements, and Josephine Hobisch for her support concerning thermal analyses and gel permeation chromatography. Britta Pfeiffer and Markus Pfitscher are gratefully acknowledged for the provision of the Spectano 100 and the measurement cell.

Thirdly, I want to give big thanks to my colleagues Robin Hofmann, Matthias Windberger, Philipp Marx, Lukas Heupl, and Inge Mühlbacher for never letting a day pass by without shared laughter and pleasantries.

Fourth, a big thanks go to my family for supporting me in my study, for the numerous good advices in difficult situations and for helping me through some stressful times.

Finally, I thank all my friends for their consistent support throughout the whole study: Lukas Heupl, Lara Strohmeier, Bettina Schweda, Elisabeth Rossegger, Hannes Kühnle, Jakob Strasser, Josef Lechner, Rene Nauschnig, Ulrike Reisinger, Werner Schlemmer und Wolfgang Fortmüller. Without you all this would have never been possible!

Table of Content

Eidesstattliche Erklärung / Statutory Declaration	i
Acknowledgement	ii
1. Introduction	1
2. Scope and Motivation.....	3
3. State-of-the-Art	4
3.1. Nanodielectrica	4
3.1.1. Dielectric Characteristics of Nanodielectrica	5
3.1.2. The Tanaka Model of Interaction Zones in Composites.....	6
3.1.3. Functionalization of Nanoparticles.....	8
3.2. Epoxy Resins	10
3.3. 2-Oxazolines	12
3.3.1. 2-Oxazoline Monomers	12
3.3.2. 2-Oxazolines with Short-Chain Substituents	13
3.3.3. 2-Oxazolines with Long-Chain Substituents	15
3.3.4. Polymerization of 2-Oxazolines	16
3.3.5. Polymeranalogous Reactions of Poly(2-oxazoline)s.....	17
3.4. Polysiloxanes	18
4. Results and Discussion.....	20
4.1. Synthesis of the Monomers Dec ⁻ Ox and NonOx	21
4.2. Synthesis of Poly(2-nonyl-2-oxazoline)- <i>stat</i> -poly(2-dec-9 ¹ -enyl-2-oxazoline) .	23
4.3. Surface Functionalization of SiO ₂ Nanoparticles	24
4.4. Preparation of the Polymer- and Nanocomposite-based Specimens.....	28
4.4.1. Preparation of Nanocomposites Based on DGEBA	28
4.4.2. Preparation of Nanocomposites Based on Di ⁻ Siloxane.....	29
4.4.3. Preparation of Nanocomposites based on pNonOx ₈₀ - <i>stat</i> -pDec ⁻ Ox ₂₀	30
4.5. Differential Scanning Calorimetry of the Polymers and the Nanocomposites .	31
4.6. Curing Kinetics of the Polymers and the Nanocomposites	32
4.6.1. Curing Kinetics of Epoxy Resins	32

4.6.2.	Curing Kinetics of Polysiloxanes	34
4.6.3.	Curing Kinetics of Poly(2-oxazoline)s	36
4.7.	Transmission Electron Microscopy of the Polymers and the Nanocomposites	38
4.7.1.	TEM Measurements of the Epoxy Resins	38
4.7.2.	TEM Measurements of the Polysiloxanes	40
4.7.3.	TEM Measurements of the Poly(2-oxazoline)s	41
4.8.	Thermal Conductivity of the Polymers and the Nanocomposites.....	42
4.8.1.	Thermal Conductivity of the Epoxy Resins	42
4.8.2.	Thermal Conductivity of Polysiloxanes.....	43
4.8.3.	Thermal Conductivity of the Poly(2-oxazoline)s	44
4.9.	Water Uptake of the Polymers and the Nanocomposites	44
4.9.1.	Water Uptake of the Epoxy Resins.....	45
4.9.2.	Water Uptake of the Polysiloxanes	45
4.9.3.	Water Uptake of the Poly(2-oxazoline)s	46
4.10.	Dielectric Characterization of the Polymers and the Nanocomposites.....	47
4.10.1.	Dielectric Characterization of the Epoxy Resins.....	47
4.10.2.	Dielectric Characterization of the Polysiloxanes	50
4.10.3.	Dielectric Characterization of the Poly(2-oxazoline)s	53
5.	Conclusions	55
6.	Abstract.....	60
7.	Kurzfassung.....	61
8.	Materials and Methods.....	62
8.1.	Used Chemicals.....	62
8.2.	Analytical Methods.....	63
8.3.	Synthesis of 2-Dec-9'-enyl-2-oxazoline	64
8.4.	Synthesis of 2-Nonyl-2-oxazoline	65
8.5.	Synthesis of Poly(2-nonyl-2-oxazoline)- <i>stat</i> -poly(2-dec-9'-enyl-2-oxazoline) .	66
8.6.	Functionalization of the Nanoparticles	66
8.7.	Preparation of the Test Specimens.....	67
8.7.1.	Epoxy Resin-based Specimens.....	67
8.7.2.	Polysiloxane-based Specimens.....	68

8.7.3. Poly(2-oxazoline)-based Specimens	68
9. References.....	69
10. Appendix.....	74
10.1. List of Abbreviations	74
10.2. List of Figures	74
10.3. List of Schemes	77
10.4. List of Tables	78

1. Introduction

Energy storage and energy transfer are among the main topics in industry as well as in research in modern days. Numerous studies are performed concerning the production and storage of energy. Besides, also another concept is of high importance: the transfer of energy. In the context of energy production, storage and transfer, most people think of copper cables, the conducting wires in transformers, or the electromagnets used in generators for the production of energy. [1]

All these different parts of the power grid have one thing in common: the use of polymers as insulating material. Polymers are used as outer layer of copper cables for energy transport and as insulators in transformers as well as generators. Common polymers for insulation materials are epoxy resins, polyesters, polyamides, polyethylene, polypropylene, ethylene vinyl acetate and silicon rubbers. [2]

With the growing amount of energy to be produced and transferred, also the requirements for the involved insulating materials are growing, such as the enhancement of permittivity, dielectric loss, thermal conductivity, breakdown strength and mechanical properties. While humidity deteriorates insulating properties, also the lowered water uptake is among those requirements. [3, 4]

In the last decades, intense research on a material class called 'nanodielectrics' has been started, which seem to fit the demands of future energy industry. This material class is defined as follows: *'[...], a nanodielectric would consist of a multicomponent dielectric possessing nanostructures, the presence of which results in the change of one or several of its dielectric properties'*. [5] Or, in other words: The term nanodielectric describes a material which consists, for example, of a polymer matrix that is filled with nanoscaled fillers; it is argued that upon the addition of nanofillers, at least one of the materials' dielectric properties such as the permittivity or dielectric loss changes.

Nanofillers are preferentially used because of their high surface area. This increase leads to different properties of a composite material compared to microcomposites or the unfilled bulk material itself. This effect is especially recognized at nanoparticles with a size of 20 nm and smaller. [6] Common nanofillers in use comprise layered silica, spherical silica, alumina, titania and (hexagonal) boron nitride. [2]

A main focus has addressed nanodielectrics with epoxy resins as polymer matrix. The reason arises from the fact that epoxy resins are widely used in industry because of their good electrical properties, good thermal properties, good mechanical properties, corrosion resistance, and easy processability. [7] Important types of epoxy resins, which are not only used in the energy sector but also for example in food packaging, are based on Bisphenol A diglycidyl ether.

Recent studies showed that monomers based on Bisphenol A have negative impact on the human health due to their similarity with the female hormone estrogen. [8, 9] Correspondingly, starting in 2020, initial regulations for the application of Bisphenol A-based resins will come into law; the European Commission has announced continued regulatory affairs in this area. [10] Therefore, alternatives for Bisphenol A-based resins have to be found.

As already mentioned herein above, polyamides as well are often used for insulating applications. The polymer class poly(2-oxazoline)s, also referred to as 'pseudo-polyamides', could be one of the possible future alternatives for insulating applications instead of an epoxy-based resins. In comparison with classic polyamides, they have the major advantage of the large variety of possible monomers. [11]

Due to the large variety of 2-oxazoline monomers, poly(2-oxazoline)s and derived copolymers with tailor-made properties can be synthesized. Depending on the monomers used, the (co-)polymers show, e.g., hydrophilic or hydrophobic behavior. Furthermore, the introduction of functional groups into the side-chains of the repetition units of the copoly(2-oxazoline)s offers many possibilities for polymeranalogous reactions of this polymer class, yielding, for example, crosslinked polymer networks.

Studies concerning the dielectric properties of nanocomposites based on crosslinked poly(2-oxazoline)s were already performed and revealed similar permittivity of the poly(2-oxazoline)s like of epoxy resins; their dielectric losses were comparably low. These studies support the idea to possibly apply poly(2-oxazoline)s as insulating material. [12, 13]

2. Scope and Motivation

Nanodielectrics are materials that are composed of a polymer matrix mixed with nanofillers. Due to the addition of the nanoparticles, the dielectric properties of the material eventually change; increased breakdown strength, permittivity and thermal conductivity are among the targeted properties. Unfortunately, the homogenous dispersion of the nanoparticles in the polymer matrices often is challenging, since their tendency to agglomerate is generally high.

Another factor, which is important for the performance of nanodielectrics, is the water uptake. This phenomenon has previously been investigated on the examples of Bisphenol A diglycidyl ether-based polymers that were filled with different kinds of nanoparticles. The different nanocomposites were stored at 30 °C and 85% humidity for 6 weeks, and the impact of the water uptake on the dielectric loss was determined. The dielectric characterization of the 'wet' nanocomposites showed significant and unfavorable increase of the dielectric loss in some of the composites. [14]

The aim of this master thesis was to determine the water uptake of different polymers filled with silica nanoparticles. In particular, and advancing the state-of-the-art knowledge, it should be investigated if the water uptake was altered if the silica nanoparticles were covalently attached to the polymer matrix. Finally, the influence of the water uptake on the dielectric properties such as thermal conductivity, permittivity, and dielectric loss, should be determined.

Hence, in this study, three different polymer classes were to be investigated, namely an epoxy/amine resin, crosslinked poly(2-oxazoline)s, and silicones. Considering poly(2-oxazoline)s as 'pseudo-polyamides', three major types of polymer-based insulating materials were chosen. These polymers were tested as (unfilled) bulk material and as composites containing nanoparticles that were either covalently bound to the network or just dispersed into it. As filler, nano-silica was chosen due to its commercial availability and high abundance of surficial Si-OH groups enabling functionalization for subsequent covalent attachment into polymer networks. This experimental set-up yielded a $3 \times 3 = 9$ -membered library, the properties of which were to be correlated with the structures of the polymers and composites.

3. State-of-the-Art

3.1. Nanodielectrics

While dielectrics possess many different features, all of them jointly contain only a few charge species and exhibit poor overlapping between the orbitals of the neighboring molecules. Therefore, charges cannot be passed on rapidly from molecule to molecule. This is the reason for their tendency to show hardly any changes under the influence of an external electromagnetic field. Nonetheless, upon application of an electromagnetic field, polarization in the material occurs. [5] Polymers are commonly used as dielectrics for insulating applications. [15] Polymer-based materials for insulation materials are epoxy resins, polyesters, polyamides, polyethylene, polypropylene, ethylene vinyl acetate and silicon rubbers. [2]

The term nanodielectric describes a material that consists, for example, of a polymer matrix that contains nanofillers (Figure 1). Upon the addition of nanofillers, at least one of the materials dielectric properties are aimed for to be altered. [5, 16] Common nanofillers for nanodielectrics are: layered silica, spherical silica, alumina, titania and boron nitride. [2]

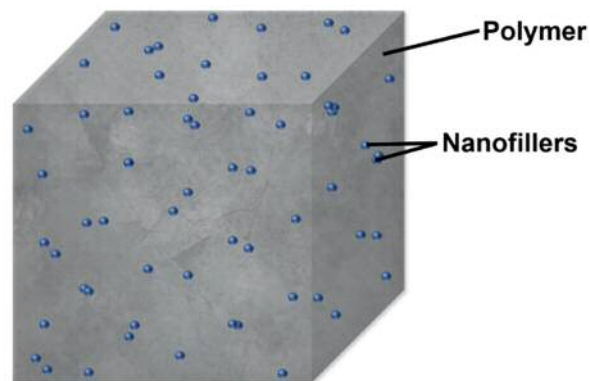


Figure 1: Schematic representation of a nanocomposite.

Nanoparticles are preferentially used in composites because of their high surface area, which often leads to different properties compared to microcomposites and the bulk material. This effect is especially pronounced in the case of nanoparticles with a size of 20 nm and smaller. [6]

As mentioned hereinabove, upon the addition of the nanofillers, the dielectric properties of the corresponding composites are expected to vary from those of the unfilled polymer. Nanoparticles are used for the fine-tuning of different properties; in most cases, however, improved insulating properties and increased thermal conductivity are targeted. [3, 4]

3.1.1. Dielectric Characteristics of Nanodielectrics

When a dielectric is exposed to an electromagnetic field E , the positive and negative charges within the material are shifted from each other. This shift leads to the formation of, e.g., dipoles, the sum of which amounts to the polarization P of the material. [17, 18] The polarization of any material is dependent on its electrical susceptibility χ_e . High electrical susceptibility indicates high polarizability of the material, while low values indicate low polarizability of the material. The polarization can be calculated as product of the permittivity of free space $\epsilon_0 = 8.854 \cdot 10^{-12} \text{ F} \cdot \text{m}^{-1}$, the material's electrical susceptibility χ_e , and the applied electromagnetic field E according to Equation (1). [19]

$$P = \chi_e \cdot \epsilon_0 \cdot E \quad (1)$$

The electrical susceptibility χ_e and the relative permittivity ϵ_r are correlated according to Equation (2).

$$\chi_e = \epsilon_r - 1 \quad (2)$$

The relative permittivity ϵ_r is defined as the relative charge storage capability of a material compared to the one of free space. The dielectric capacitance D of free space is given by the following Equation (3):

$$D = \epsilon_0 \cdot E + P \quad (3)$$

From those three equations, the following relationship for dielectric materials can be derived (Equation (4)):

$$D = \epsilon_0 \cdot \epsilon_r \cdot E \quad (4)$$

Since E and ϵ_0 are constants, the dielectric capacitance D is dependent on the relative permittivity ϵ_r , and therefore on the polarization P , which explains the importance of the relative permittivity as key criterion for dielectric materials. [19]

The relative permittivity of a material consists of two parts: the real part ϵ' and the imaginary part ϵ'' . Whereas the real part of the permittivity ϵ' describes the charge stored in material, the imaginary part of the permittivity ϵ'' describes the loss of electrical energy within a material. The ratio between those two parts is called the dielectric loss or loss factor $\tan\delta$ (Equation (5)). [20, 21]

$$\tan\delta = \frac{\epsilon''}{\epsilon'} \quad (5)$$

The dielectric loss quantifies the charge losses of a material. An ideal conductor would have a dielectric loss of ∞ , an ideal insulator would have a dielectric loss of zero. Hence, high values of the dielectric loss describe a high amount of charges lost, which decreases the insulating properties of a material. Materials that are considered as good dielectrics show values $\tan\delta \ll 1$ at the industrial standard of 50 Hz. [12]

As mentioned hereinabove, upon the addition of nanofillers, the dielectric properties of the corresponding composite and the unfilled polymer might differ. Nelson et al. performed studies on epoxy-based resins filled with TiO_2 nano- and microparticles [16, 22-25]. They concluded that the difference in the properties of nanocomposites was due to the interaction zones, which are present between the polymer matrix and the nanoparticles. In fact, epoxy resins filled with nanoscaled TiO_2 showed different properties than epoxy resins filled with microscaled TiO_2 . The assumption was drawn that the high surface area of nanoparticles has a major impact on the dielectric properties of a nanocomposite. Furthermore, it was concluded that the improvement of dielectric properties was due to a control of internal charges in the bulk via interaction zones, partially suppressing interfacial polarization.

3.1.2. The Tanaka Model of Interaction Zones in Composites

For the description of the interaction zones between the polymer matrix and nanofillers, the Tanaka Model was proposed (Figure 2). This model consists of polymeric multi-layer structures surrounding the nanoparticles. Three layers and an additional electric double layer overlapping these three are described. [26]

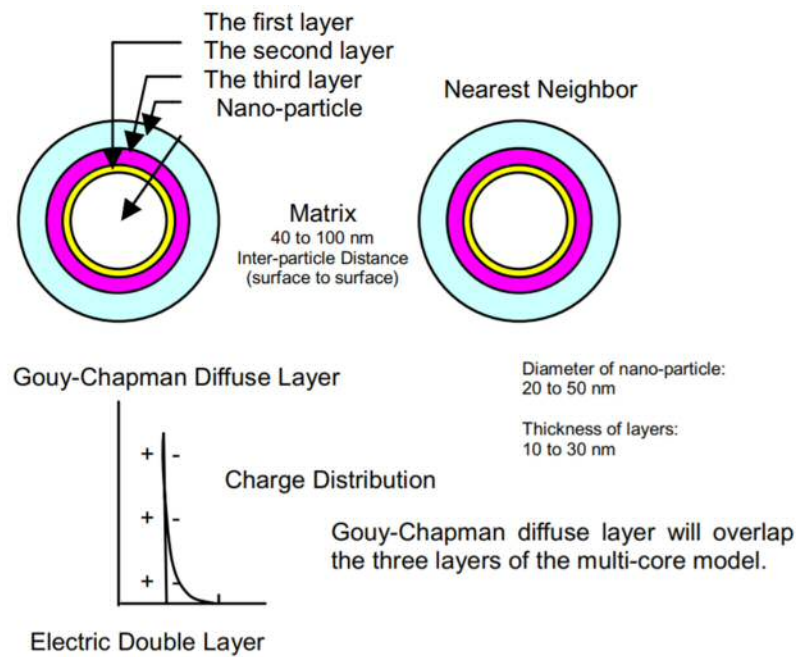


Figure 2: Multi-core model of nanoparticle-polymer interactions proposed by Tanaka et al. [26]

The nanoparticles are surrounded by the first layer, also called the bonded layer. This layer is bonded tightly to the nanoparticle's surface, and in case coupling agents or similar were used, also tightly bonded to organic substances. The second layer, or bound layer, describes the interfacial region between the polymer chains and the nanoparticles surface. The polymer chains interact with the nanoparticles surface and/or can be strongly bound to it. The third layer, or loose layer, is the region of polymer chains, which are still affected concerning their conformation and mobility, but are not in direct contact to the nanoparticle's surface. [26]

The thickness of the layers strongly depends on the kind of polymer and nanoparticles used. If nanoparticles are incorporated into a polymer matrix, different cases are possible. Depending on the polymer and nanoparticle, different interactions and, correspondingly, structural orientations can occur (Figure 3). If the polymer and the nanoparticle hardly interact at all, high interspaces between the two components are formed, leading to an increase of the layer's diameter. Electrostatic interactions or van-der-Waals interactions between the two components lead to much lower diameters. [26, 27] Another possibility is the covalent embedment of nanoparticles into a polymer network if the polymer forms covalent bonds with the

nanoparticles surface, which yields very tight networks and low diameters for the layers of the multi-core model. [26, 27] Nelson et al., for example, functionalized SiO₂ particles with triethoxyvinylsilane for the introduction of double bounds on the surface of the nanoparticles. Due to this strategy, covalent embedment of the SiO₂ nanoparticles in low-density-poly-ethylene was achieved. [28]

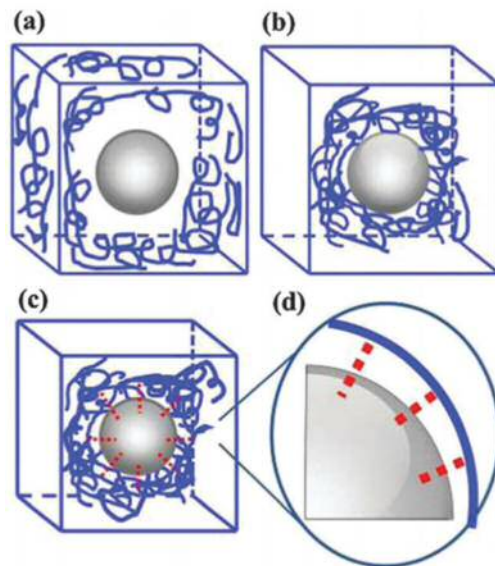


Figure 3: Illustration of the different interactions between a nanoparticle and a polymer matrix: (a) Nearly no interaction. (b) Electrostatic or van-der-Waals interactions that lower the interspace. (c, d) Covalent bonds between the nanoparticle and the polymer matrix. [27]

3.1.3. Functionalization of Nanoparticles

For the functionalization of nanoparticles, an 'active' surface bearing functional groups is desirable. In the case of oxides, for example alumina and silica (Figure 4), the presence of hydroxy groups on their surface enables functionalization reactions in straightforward fashion. In the case of inert nanoparticles, as for example boron nitride (Figure 4), a functionalization is more challenging since the 'activation' of the surface would be necessary in a prior step. A very well-known common method for the functionalization of silica is the reaction with trimethylchlorosilane TMCS or hexamethyl-disilazane HMDS, yielding tetramethylsilyl TMS groups on the surface of a nanoparticle (Scheme 1). In both cases, the surface of silica can be made more hydrophobic, which is used for the pre-treatment of silicon wafers. [29]

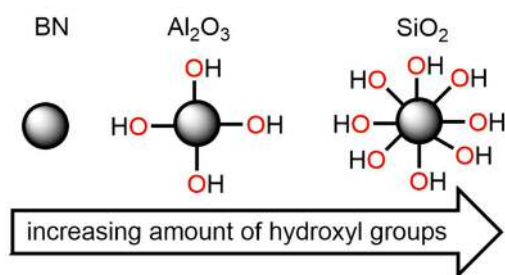
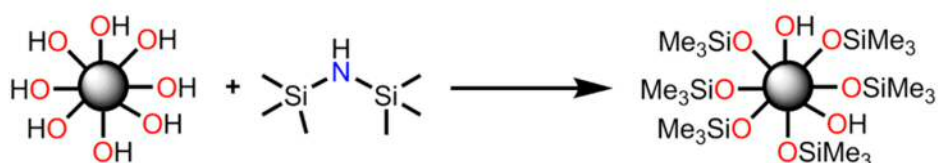


Figure 4: Amount of hydroxy groups present on a nanoparticle's surface.



Scheme 1: Functionalization of a silica surface with HMDS. [29]

Another method for the surface functionalization of nanoparticles is the reaction with silane coupling agents, which was first introduced by Plueddemann et al. (Figure 5). [30] Firstly, the silane coupling agents are hydrolyzed, yielding unstable hydroxides. These hydroxides participate in the typical condensation reaction, which is widely used for the industrial production of siloxanes. Afterwards, the remaining hydroxy groups react with the hydroxy groups present on the nanoparticles under the elimination of water. Nowadays, many silane coupling agents and functionalization strategies are (commercially) available, [31] to name a few examples:

- Zhao et al. used aminopropyl-trimethoxysilane APTMS and 3-isocyanatopropyl-trimethoxysilane for the functionalization of TiO_2 . [31]
- Ahangaran et al. functionalized the surface of Fe_3O_4 -coated SiO_2 particles with vinyl-triethoxysilane VTES and observed decreased agglomeration. [32]
- Prado et al. increased the hydrophobicity of Al_2O_3 nanoparticles by the modification with [2-(3,4-epoxycyclohexyl)-ethyl]-trimethoxysilane. [33]
- Iijima et al. used three different silane coupling agents for the surface functionalization of TiO_2 nanoparticles. By varying the amounts of different coupling agents, stable dispersion could be obtained for various organic solvents. [34]

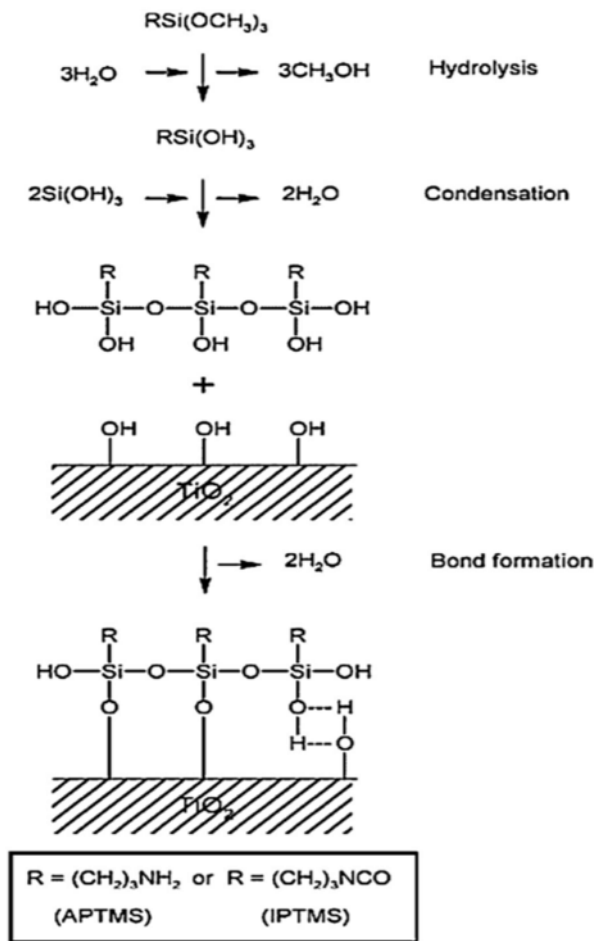


Figure 5: Functionalization of a nanoparticle's surface with a silane coupling agent. [31]

3.2. Epoxy Resins

An important polymer class constituting the basis for lots of different insulating materials are resins based on epoxides. All of these resins have one structural function in common: the epoxy ring (Figure 6). [35] The epoxy ring easily undergoes ring-opening reactions via S_{N1} or S_{N2} mechanism after the attack by a nucleophile. The reason for this high reactivity is the high ring strain. [36]

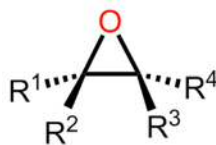


Figure 6: Structure of the epoxy functionality.

In addition to the high reactivity of the monomers, the corresponding epoxy resins show a lot of advantages such as good electrical properties, good thermal properties, good mechanical properties, corrosion resistance and easy processability. On the other hand, drawbacks like high water uptake and the brittle nature of the crosslinked structures can be bottlenecks for some applications. [7, 37-38] Different monomers are used in insulating applications. One important example are epoxy resins based on Bisphenol A diglycidyl ether DGEBA (Figure 7). [39]

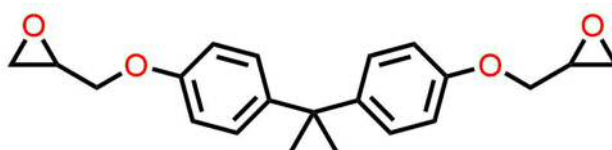
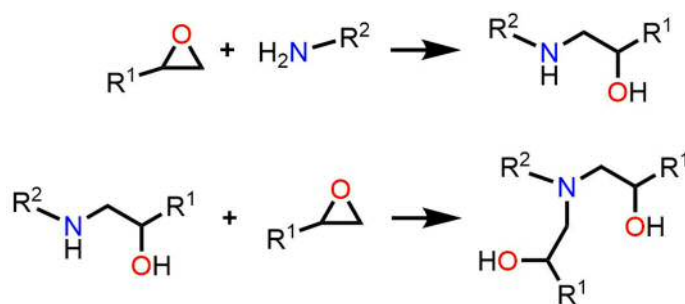


Figure 7: Structure of DGEBA.

The epoxy rings of DGEBA can react in ring-opening fashion with so-called hardeners. Different hardeners are currently used in industry for the crosslinking reaction of DGEBA, mostly based on either anhydrides or amines. The crosslinking reaction for an amine-based hardener is shown in Scheme 2. [39]



Scheme 2: Crosslinking reaction of an epoxide cured with an amine-based hardener.

In case of DGEBA-based epoxy resins, different kinds of nanofillers are already under intense investigation aiming to improve the dielectric properties of the corresponding materials. Danikas et al. showed that the flashover voltage was increased upon the addition of various amounts of TiO_2 nanofillers (compared to the unfilled resin). [40] Furthermore, the flashover voltage was the highest for a filler

content of 5 wt.-%, leading to the assumption that a too high or too low filler content can both decrease the flashover voltage again.

Couderc et al. added boron nitride and silica nanoparticles to an epoxy resin and observed the simultaneous occurrence of decreased glass-transition temperatures and increased heat capacity. [41] Gu et al. observed an increase of the thermal conductivity in epoxy resins by the addition of functionalized graphite nanoplatelets. In fact, with a filler content of 30 wt.-%, the thermal conductivity could be increased from 0.20 to $1.70 \text{ W}\cdot\text{m}^{-1}\text{K}^{-1}$. [42]

Iyer et al. observed improvements concerning the dielectric loss of epoxy resins filled with micro- and nano-scaled silica particles. [43] Danikas et al. reported the increase of breakdown strength and the decrease of electrical trees' growth if nanofillers were homogeneously dispersed in an epoxy resin. They concluded that the nanoparticles acted as barriers hindering the growth of electrical trees and, therefore, increasing the breakdown strength of a nanocomposite. [44] Singha et al. observed that the addition of low amounts of oxide-based nanofillers such as TiO_2 and ZnO to epoxy resins resulted in a decrease of the dielectric loss and the permittivity at low loadings (compared to the unfilled epoxy resins). [45]

3.3. 2-Oxazolines

Aside from other polymers, also polyamides are often used for insulating applications. Polymers based on 2-oxazolines can be described as 'pseudo-polyamides' since their amide functionality is present in the side-chain of each repetition unit. [46, 47] Hence, also this polymer class could be a possible alternative for insulation applications. Studies concerning the dielectric properties of nanocomposites based on this material were already performed, showing a permittivity similar to those of epoxy resins, and low dielectric losses of up to 0.093. [12, 13]

3.3.1. 2-Oxazoline Monomers

In general, the monomers for this polymer class is based on a five-membered ring, in which a nitrogen atom occupies position 1 and an oxygen atom position 3. A double

bond among the nitrogen atom and the carbon atom at position 2 is present in the ring. On the carbon atom at position two, many different substituents are possible, leading to a large variety of different monomers (Figure 8). [11]

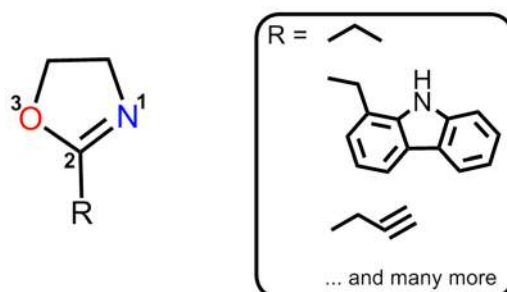


Figure 8: Monomer structure of 2-oxazolines with possible substituents. [11]

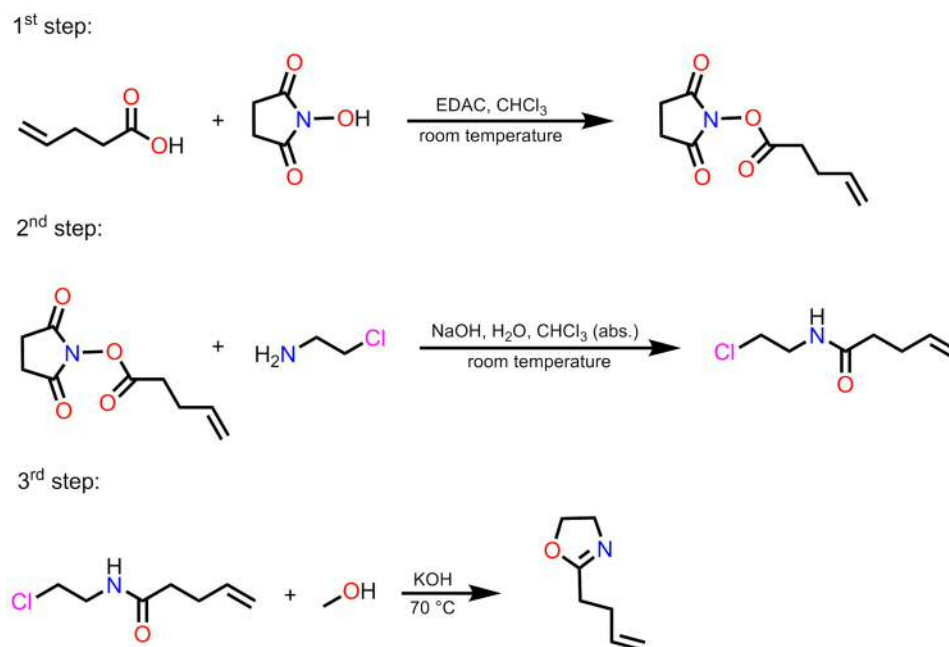
The first 2-oxazoline monomer was synthesized by Gabriel in 1889. [48] Today, different synthesis routes are known for 2-oxazolines with different substituents. Synthesis routes differ for 2-oxazolines with short-chain or long-chain substituents. In the following chapters, syntheses are described for various 2-oxazoline monomers.

3.3.2. 2-Oxazolines with Short-Chain Substituents

In general, with short-chain substituents, side-chains with four or less carbon atoms are described. For the synthesis of such 2-oxazoline monomers, two main strategies will be introduced: the synthesis according to Schlaad and the synthesis according to Hoogenboom. Both synthesis strategies are explained on the example of 2-but-3'-enyl-2-oxazoline as monomer. [49, 50]

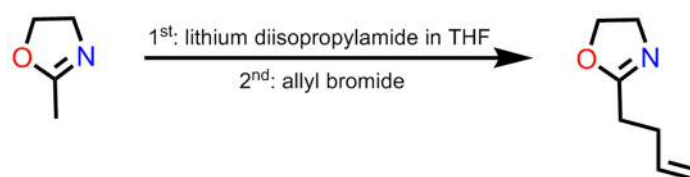
Synthesis according to Schlaad: The three-step synthesis starts with the educts pent-4-enoic acid and *N*-hydroxysuccinimide (Scheme 3). In the first step, pent-4-enoic acid is converted into the active ester *N*-succinimidyl-pent-4-enoat. This active ester is subsequently reacted with 2-chloroethane-1-amine under ring-opening, yielding the amide *N*-(2-chloroethyl)-pent-4-enamide. In the last reaction step, the amide reacts with methanol in the presence of potassium hydroxide, yielding the targeted

monomer 2-but-3'-enyl-2-oxazoline. Major drawbacks of this synthesis route, however, are low yields, the use of halogenated solvents, and long reaction times. [49]



Scheme 3: Three-step synthesis of 2-but-3'-enyl-2-oxazoline according to Schlaad.

Synthesis according to Hoogenboom: In this synthesis, 2-methyl-2-oxazoline is added dropwise to a cooled solution of lithium diisopropylamide ($-78\text{ }^{\circ}\text{C}$) under nitrogen atmosphere (Scheme 4). Allyl bromide is added, and the mixture is slowly warmed up to room temperature. After stirring overnight, the reaction mixture is quenched with methanol. Volatile components are removed by evaporation, yielding the crude product. Subsequently, dissolving in dichloromethane, washing with water and brine and vacuum distillation yields the purified 2-but-3'-enyl-2-oxazoline. [50]

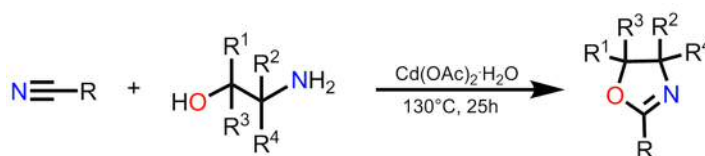


Scheme 4: Synthesis of 2-but-3'-enyl-2-oxazoline according to Hoogenboom.

3.3.3. 2-Oxazolines with Long-Chain Substituents

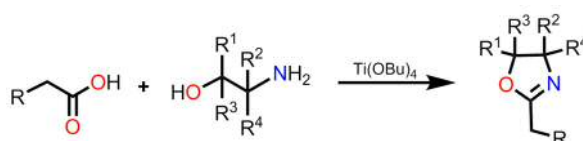
In the case of 2-oxazolines with long-chain substituents, two main strategies will be introduced as well: the synthesis according to Witte and Seeliger and the synthesis according to the Henkel patent. [51, 52]

Synthesis according to Witte and Seeliger: 2-Aminoalcohols are reacted with nitriles under the presence of a metal catalyst, for example cadmium acetate dihydrate (Scheme 5). The reaction is performed under inert atmosphere and temperatures above 130 °C. The addition of solvents is not necessary. After 25 h of reaction time, the pure product can be obtained by distillation. [51]



Scheme 5: Synthesis of 2-oxazoline monomers according to Witte and Seeliger.

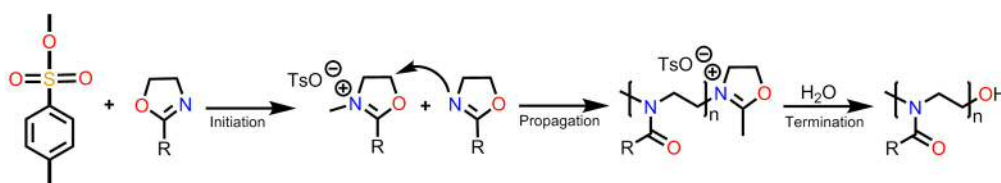
Synthesis according to the Henkel-patent: A fatty acid with at least six carbon atoms is reacted with ethanolamine under the presence of a titanium catalyst, for example titanium butoxide (Scheme 6). The pure product can be obtained via distillation. [52] Compared to the catalyst suitable for the synthesis according to Witte and Seeliger, these catalysts are less dangerous for the environment, which is a major advantage of this synthesis route. Another major advantage is the fact that the fatty acids used for the synthesis can be won from renewable resources. For the synthesis of 2-deceny-2-oxazoline or 2-nonyl-2-oxazoline, undecenoic acid or decanoic acid is used, which can be produced from castor oil or coconut oil. Ethanolamine can be won from the amino acid serine. [53]



Scheme 6: Synthesis route of 2-oxazoline monomers according to the Henkel patent.

3.3.4. Polymerization of 2-Oxazolines

The first polymerizations of 2-oxazoline monomers were performed in the 1960s by four independent research groups. [54-57] A big disadvantage of polymer syntheses based on 2-oxazolines were the long reaction times up to several days. With the development of microwave reactors, these reaction times could be reduced a lot. Since a microwave reactor offers autoclave conditions, reactions can be performed at much higher temperature and, consequently, the reaction times can be reduced: The synthesis of poly(2-ethyl-2-oxazoline) with PD = 100 (Scheme 7) under conventional reflux lasts 60 h, due to the boiling point of acetonitrile of 82 °C. If this reaction is performed in a microwave reactor, higher temperatures can be achieved. The reaction time for the synthesis of poly(2-ethyl-2-oxazoline) with PD = 100 could be reduced by a factor of 350, leading to a reaction time of only 1 min at 190 °C. [58]



Scheme 7: Cationic ring-opening polymerization of 2-oxazolines with methyl tosylate as initiator.

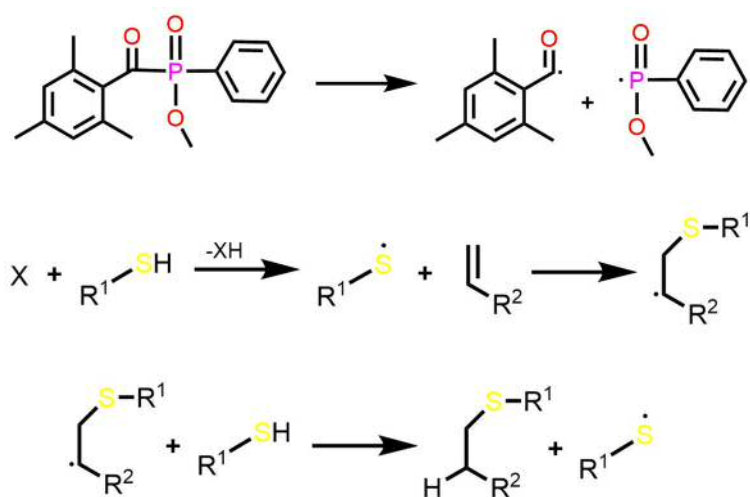
Literature states that the polymerization of 2-oxazolines follows a pseudo-living cationic ring-opening polymerization. This means that the kinetic constant of the initiation step is larger than that of the propagation step. Moreover, all active chains grow with the same rate, and there are no termination or chain-transfer reactions. These factors lead to a defined chain length of the synthesized polymers. Furthermore, the mechanism enables the polymerization of block copolymers and gradient copolymers, as well as statistical copolymers. [59, 60] Methyl tosylate can be used as initiator, as it activates the 2-oxazoline ring, which then can be attacked by another monomer (Scheme 7). [59] Wiesbrock et al. showed that the initiation reaction is regioselective. The π -electrons along the N-C-O bond are delocalized, leading to a nucleophilic attack of the nitrogen atom on a carbon atom of another (activated) 2-oxazoline ring. [61]

3.3.5. Polymeranalogous Reactions of Poly(2-oxazoline)s

As already mentioned, on the carbon atom at position two of 2-oxazoline monomers, many different substituents may be attached, leading to a large variety of different monomers. Consequently, this large variety of monomers offers many possibilities of polymeranalogous reactions. A widely used polymeranalogous reaction is the thiol-ene click reaction. In general, click chemistry has major advantages compared to other reactions:

- a high selectivity as well as regio- and stereospecificity,
- absence of dangerous side-products,
- high conversion, and
- mild reaction conditions and insensitivity against water and oxygen. [62]

In most cases, the thiol-ene click reaction is used for the crosslinking of polymers, like in the case of poly(2-oxazoline)s containing double bonds, yielding highly crosslinked polymer networks. [63] For the start of the thiol-ene click reaction, an initiator is needed, either a thermal radical starter or a UV-induced radical starter. [64] One potential radical starter is the photoinitiator TPO-L, the reaction of which can be started with UV illumination (Scheme 8).



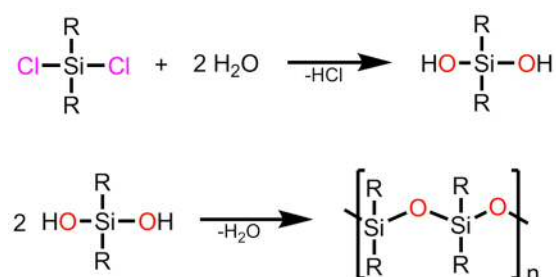
Scheme 8: Mechanism of the thiol-ene click reaction.

The UV irradiation leads to decomposition of the photoinitiator TPO-L, yielding two radicals. These two radicals can abstract a proton from the thiol functionality, yielding a thiyl radical. In the next step, the double bond is attacked under the formation of a thioether (sulfur-carbon bond). The resulting radical at the carbon atom can abstract a proton from the thiol functionality, regaining the thiyl radical. Via this reaction, the double bonds of poly(2-oxazoline)s can react with a thiol-based crosslinker, leading to a highly crosslinked polymer network. [64]

3.4. Polysiloxanes

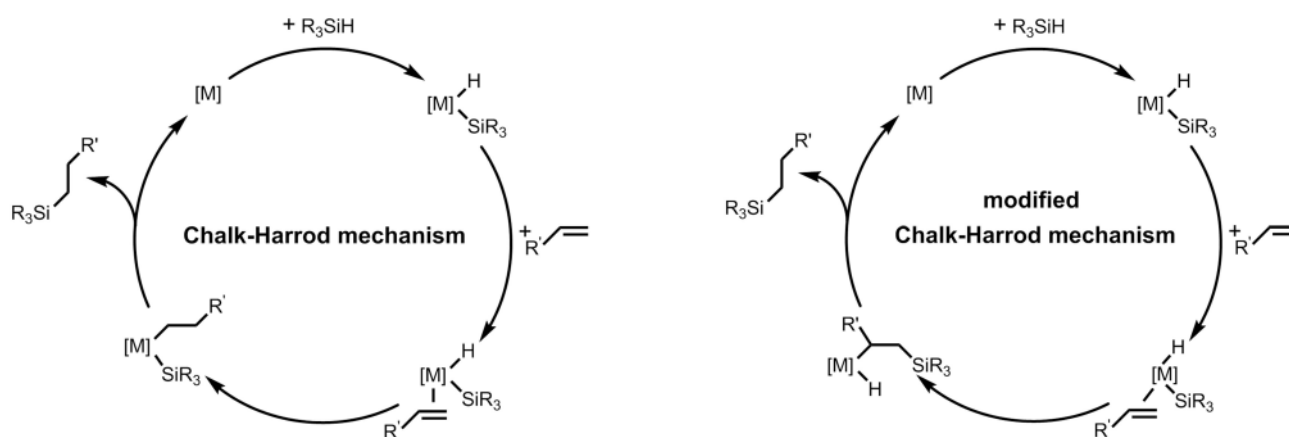
Another polymer class, suitable for insulating applications, are polysiloxanes. These polymers consist of $-\text{SiR}_2\text{-O}-$ repetition units. The high stability of the Si-O bond leads to high thermal stability, and, therefore, a potential application range of the corresponding dielectric over a broad range of temperatures. The side-groups of the polysiloxanes can be used for crosslinking of the polymer chains; moreover, different network densities can be achieved. These variation possibilities enable the production of liquids such as silicone oil as well as solid polymers such as silicon rubbers. [65, 66] For the polymerization of the different polymers, two main reaction types are widely used, polycondensation and hydrosilylation.

Polycondensation. For the polycondensation reaction, chlorosilanes are used as educts, which are synthesized via the Müller-Rochow process. [67] In the first step, the chlorosilanes react with water under elimination of HCl, yielding unstable hydroxides. These hydroxides then undergo condensation reactions, building up the polymeric chains (Scheme 9). [65] By mixing di-, tri- and tetra-substituted chlorosilanes, different degrees of crosslinking can be achieved.



Scheme 9: Mechanism of the polycondensation of polysiloxanes. [65]

Hydrosilylation. In case of the hydrosilylation, a hydride-substituted siloxane is reacted with a C=C double bond in the presence of (commonly) a platinum catalyst. [66] In industry, the Karstedt catalyst is highly used due to its high turnover number TON and turnover frequency TOF. [68] This double bond can be present on a functionalized siloxane, but also the addition of organic polymers is possible with this reaction. Two different mechanism are proposed for the hydrosilylation (Scheme 10), the Chalk-Harrod mechanism and the modified Chalk-Harrod mechanism. [69, 70]



Scheme 10: Mechanism of the hydrosilylation of polysiloxanes. [69, 70]

Aside from the hydrosilylation reaction, also the already described thiol-ene click reaction can be performed with vinyl-functionalized silicones.

4. Results and Discussion

The aim of this master thesis was to determine the water uptake of different polymers filled with silica nanoparticles. In particular, and advancing the state-of-the-art knowledge, it should be investigated if the water uptake was altered if the silica nanoparticles were covalently attached to the polymer matrix. Finally, the influence of the water uptake on the dielectric properties such as thermal conductivity, permittivity, and dielectric loss, should be determined. Hence, in this study, three different polymer classes were to be investigated:

- an epoxy resin based on Bisphenol A diglycidyl ether DGEBA to be cured with diethylenetriamine DETA,
- the poly(2-oxazoline) pNonOx₈₀-*stat*-pDec⁺Ox₂₀ based on 2-nonyl-2-oxazoline NonOx and 2-decenyl-2-oxazoline Dec⁺Ox, both of which can be synthesized according to the Henkel-patent, [52] and
- a polysiloxane based on 1,3-divinyltetramethyldisiloxane Di⁺Siloxane to be cured with a mixture of 2,2'-(ethylenedioxy)diethanethiol and trimethylolpropane-tris(3-mercaptopropionate).

These polymers were tested as (unfilled) bulk material and as composites containing nanoparticles that were either covalently bound to the network or just dispersed into it. As filler, nano-silica with a stated size of 5-15 nm was chosen as nanofiller. The hydroxy groups on the surface of the SiO₂ nanoparticles were functionalized with mercaptopropyl-trimethoxysilane MPTMS, yielding SiO₂-MPTMS nanoparticles. These nanoparticles were covalently embedded into every of the three polymer matrices.

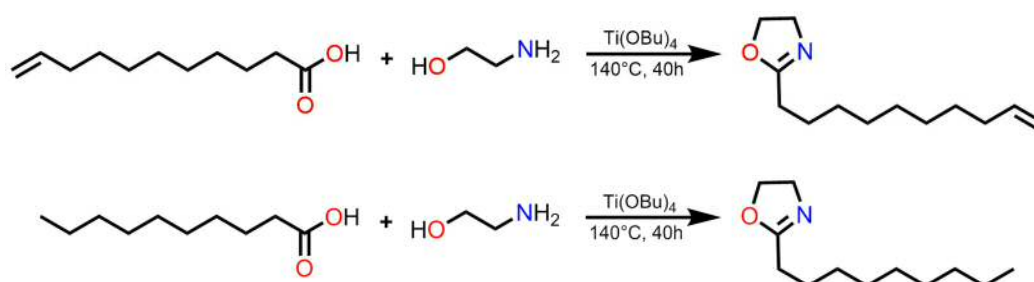
This experimental set-up yielded a 3 x 3 = 9-membered library, the properties of which were to be correlated with the structures of the polymers and composites. (Table 1). The difference between nanocomposites filled with commercial SiO₂ and filled with SiO₂-MPTMS was characterized using differential scanning calorimetry and transmission electron microscopy. Time-dependent water uptake was investigated and dielectric characterization of the test specimen was performed in dry and wet state.

Table 1: Different kind of polymers and composites used in this investigation.

Polymer ↓ / Filler →	Unfilled	5 wt.-% SiO ₂	5 wt.-% SiO ₂ -MPTMS
DGEBA	Epoxy Resin 1	Epoxy Resin 2	Epoxy Resin 3
pNonOx ₈₀ -stat-pDec ⁻ Ox ₂₀	Polyoxazoline 1	Polyoxazoline 2	Polyoxazoline 3
Di ⁻ Siloxane	Polysiloxane 1	Polysiloxane 2	Polysiloxane 3

4.1. Synthesis of the Monomers Dec⁻Ox and NonOx

The synthesis of both monomers was performed according to the Henkel-Patent. [52] Therefore, a fatty acid was reacted with ethanolamine under the presence of the catalyst Ti(OBu)₄ (Scheme 9). In case of Dec⁻Ox, undecenoic acid was used, whereas for NonOx, decanoic acid was the educt.



Scheme 11: Synthesis of 2-dec-9'-enyl-oxazoline and 2-nonyl-oxazoline according to Henkel-Patent

For both reactions, the reaction mixture was stirred for 40 h under reflux before the product was obtained from vacuum distillation and subsequent column chromatography in CHCl₃ with yields of 68.1% for Dec⁻Ox and 53.3% for NonOx.

In the ¹H-NMR spectra of Dec⁻Ox (Figure 9), the signals at δ = 1.23, 1.53, 1.93 and 2.16 represent the hydrogen atoms of the saturated part of the side-chain (marked as 4, 4', 5 and 6). Furthermore, the signals of the hydrogen atoms of the double bond are identified in higher ppm regions at δ = 4.84 and 5.72 ppm (marked as 1 and 2). The four hydrogen atoms of the 2-oxazoline pentacycle can be identified at δ = 3.71 and 4.11 ppm (marked as 3 and 3').

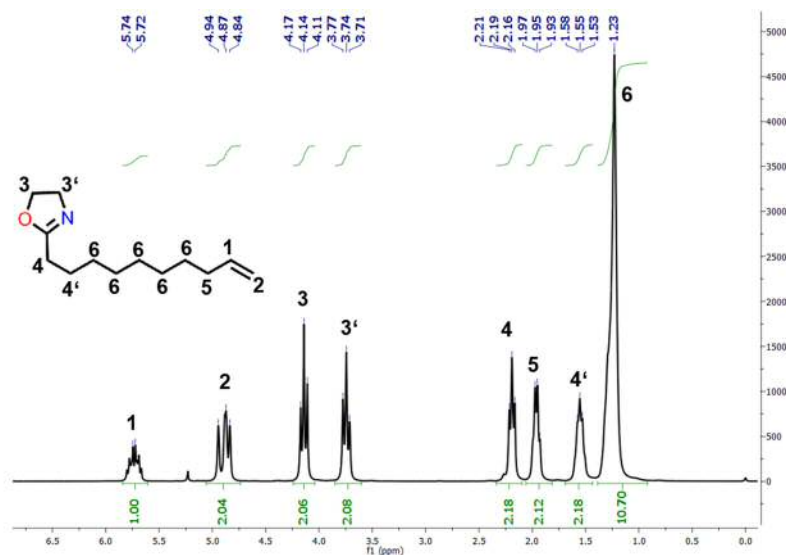


Figure 9: ¹H-NMR spectrum of Dec⁺Ox with signals assigned to the chemical structure.

In the ¹H-NMR spectra of NonOx (Figure 10), the signals at $\delta = 0.78$, 1.19, 1.53 and 2.17 ppm represent the hydrogen atoms of the saturated part of the side-chain (marked as 2, 2', 3 and 4). The four hydrogen atoms of the 2-oxazoline ring can be identified at $\delta = 3.71$ and 4.11 ppm (marked as 1 and 1').

For both monomers, the NMR-measurements revealed high purity of the products.

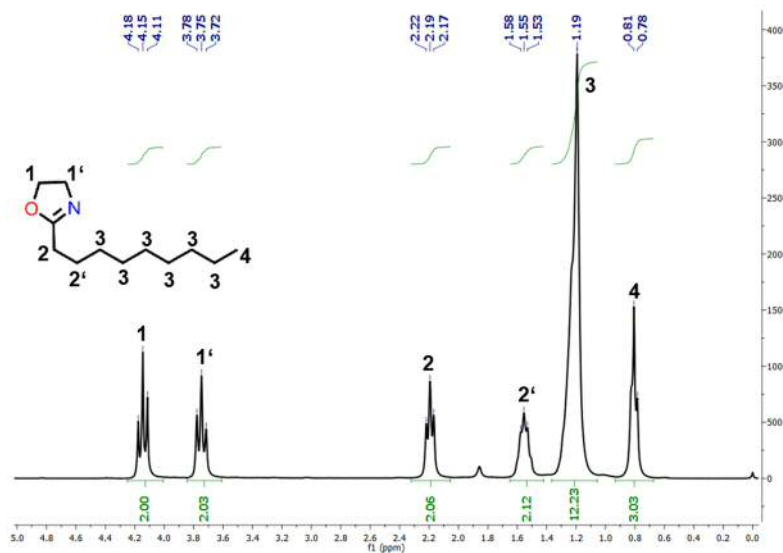
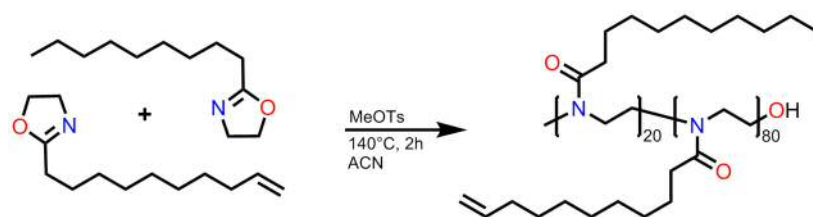


Figure 10: ¹H-NMR spectrum of NonOx with signals assigned to the chemical structure

4.2. Synthesis of Poly(2-nonyl-2-oxazoline)-*stat*-poly(2-dec-9'-enyl-2-oxazoline)

The copolymerization of Dec⁻Ox and NonOx was performed via microwave-assisted synthesis. 20 equiv. of Dec⁻Ox and 80 equiv. of NonOx were mixed; as initiator, methyl-tosylate was added; as solvent, acetonitrile was used. The copolymerization, which followed a cationic ring opening mechanism, yielded the copolymer pNonOx₈₀-*stat*-pDec⁻Ox₂₀ (Scheme 10).



Scheme 12: Microwave-assisted synthesis of the copolymer pNonOx₈₀-*stat*-pDec⁻Ox₂₀.

The product was obtained as white powder after rotary evaporation in a yield of $\geq 99\%$. The ¹H-NMR spectra of pNonOx₈₀-*stat*-pDec⁻Ox₂₀ in CDCl₃ is shown in Figure 11.

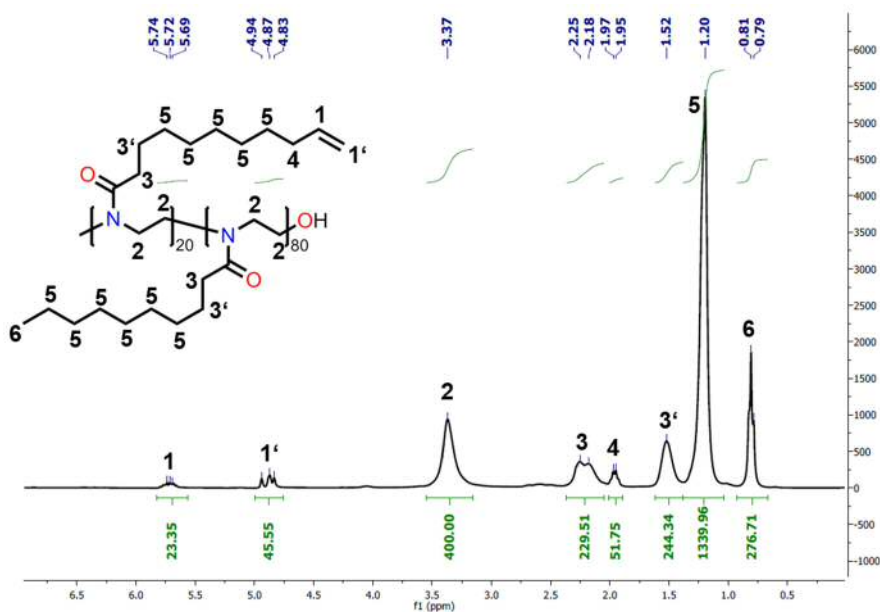


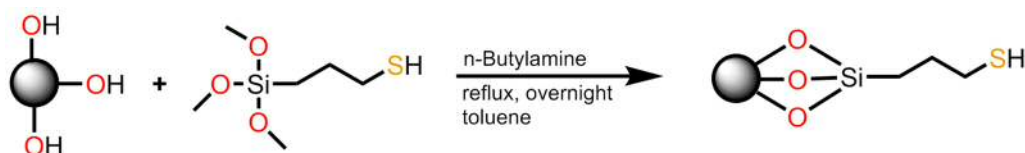
Figure 11: ¹H-NMR spectrum of pNonOx₈₀-*stat*-pDec⁻Ox₂₀ with signals assigned to the chemical structure.

At $\delta = 0.79, 1.20, 1.52, 1.95$ and 2.18 ppm (Figure 11), the signals for the hydrogen atoms that belong to the saturated parts of the two different side chains can be identified (marked as 3, 3', 4, 5, and 6). The signals of the hydrogen atoms of the double bond in the side chain are identified in the higher ppm region at $\delta = 4.83$ and 5.69 ppm (marked as 1 and 1'). The hydrogen atoms of the polymer main chain can be identified at $\delta = 3.77$ ppm (marked as 2). Assuming hundred repetition units, the integral of peak 2 was set to 400. The sum for the peaks 1 and 1' amounts to 68.90, while the integral of peak 6 has a value of 276.71, giving a ratio of 1:4 for the two monomers.

Since it is known that the copolymerization of 2-oxazolines follows a pseudo-living cationic ring-opening polymerization, the kinetic constant of the initiation step is significantly larger than that of the propagation step. Moreover, all active chains grow with the same speed, and there are no termination or chain-transfer reactions. All these factors lead to a defined chain length of the polymer, which is manifested in a dispersity index of 1.31.

4.3. Surface Functionalization of SiO₂ Nanoparticles

For the functionalization of commercially available SiO₂ nanoparticles, the nanoparticles were dispersed in toluene. After adding the functionalizing agent MPTMS and *n*-butylamine, which acts as catalyst, the dispersion was stirred under reflux for 5 h (Scheme 11). After centrifugation and drying, the SiO₂-MPTMS nanoparticles were obtained as white powder. Subsequent IR measurements clearly show the difference among the SiO₂-MPTMS nanoparticles and the commercial ones (Figure 12).



Scheme 13: Functionalization of the surface of SiO₂ nanoparticles.

The following peaks can be identified in the IR (Figure 12), namely the OH group at 3264 cm^{-1} (1), the Si-O-Si stretching vibration at 1061 cm^{-1} (2), the Si-OH stretching at 959 cm^{-1} (3) and the Si-O-Si bending at 806 cm^{-1} (4). [71] The main difference between the two nanoparticles can be seen at peak 1: Whereas the OH and water content is high for the commercial SiO_2 nanoparticles, no OH groups or surface-bonded water can be seen in case of the SiO_2 -MPTMS nanoparticles.

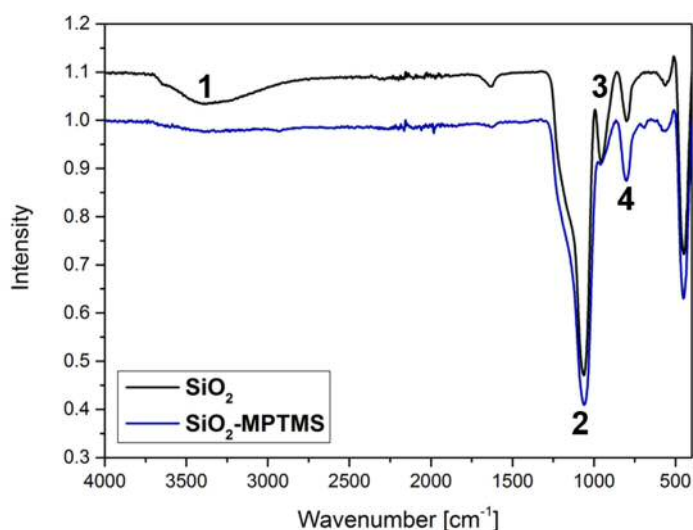


Figure 12: Infrared spectra of the commercially available SiO_2 nanoparticles (black) and the SiO_2 -MPTMS nanoparticles (blue).

Thermogravimetric analysis was performed for both nanoparticles (Figure 13).

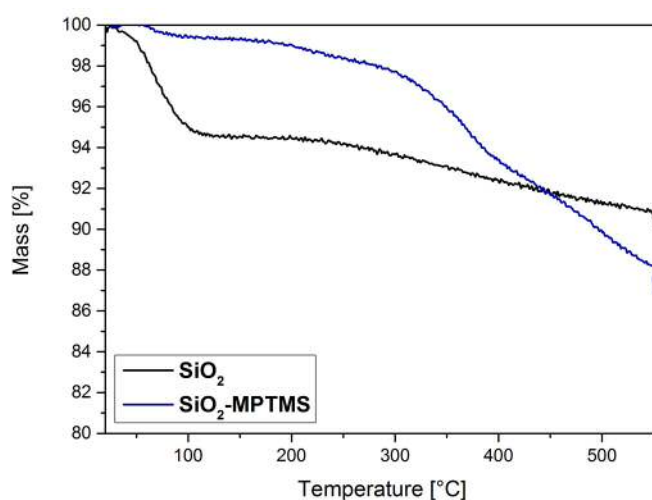


Figure 13: Thermogravimetric analysis of the commercial SiO_2 nanoparticles (black) and the SiO_2 -MPTMS nanoparticles (blue).

In case of the commercial SiO₂ nanoparticles (Figure 13), the mass decrease starts at around 90 °C. This is due to the desorption of surface-adsorbed water, leading to a weight loss of 8.8%. In comparison, the SiO₂-MPTMS shows less weight loss in the region up to 200 °C, due to the lower number of hydroxy groups on the surface, and consequently a lower amount of surface-adsorbed water. The weight loss in this region is only about 1%. When heating above 250 °C, the mass starts to decrease in a second step with a total weight loss of about 10%. The second weight loss step is due to cleavage of the functionalizing agent, also explaining the higher weight loss in percentage since the cleaved off parts have a higher molar mass compared to water.

In addition to the thermogravimetric analysis, also pyrolysis coupled with a GC-MS was performed. After heating at 500 °C for 2 min, mass spectra with retention times of up to 30 min were recorded (Figure 14).

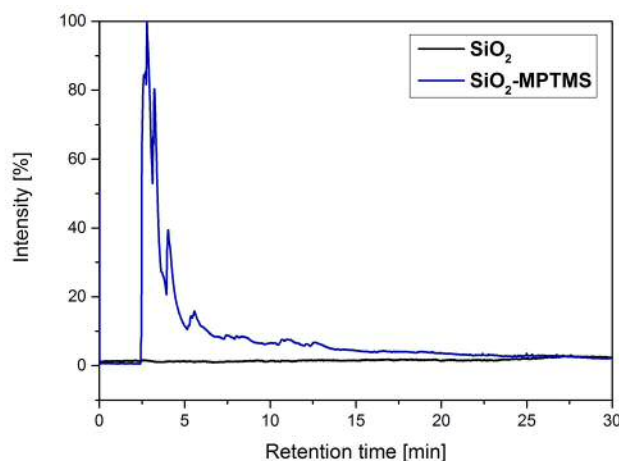
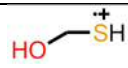
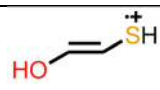
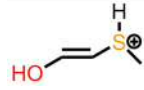


Figure 14: Pyrolysis of the commercial SiO₂ nanoparticles (black) and the SiO₂-MPTMS nanoparticles (blue).

In the case of the commercial SiO₂ nanoparticles, no pyrolysis/decomposition products were transferred to the GC-MS. This is different for the SiO₂-MPTMS nanoparticles due to the cleavage of the functionalizing agent from the nanoparticles surface. In Table 2, the different retention times are given with the according mass-to-charge ratios, as well as the suggested structures. The functionalizing agent can be cleaved off at different C-atoms and react with water and hydroxy groups, leading to the suggested structures.

Table 2: Retention times, the mass-to-charge ratio, and suggested structures of the cleaved off species.

Retention time	Mass-to-charge ratio	Suggested structures
2.62 min	64	
2.81 min	76	
4.03 min	91	

For further characterization, zeta-potential measurements of the commercial SiO₂ and the SiO₂-MPTMS nanoparticles were performed (Figure 15). The isoelectric points for both nanoparticles were calculated from the fitted trendline, yielding pH = 0.92 for commercial SiO₂ and pH = 0.73 for SiO₂-MPTMS. The similarity of the isoelectric points is due to the similar chemical behavior of hydroxy- and thiol-functionalities. This observed trend coincides with literature data. [72]

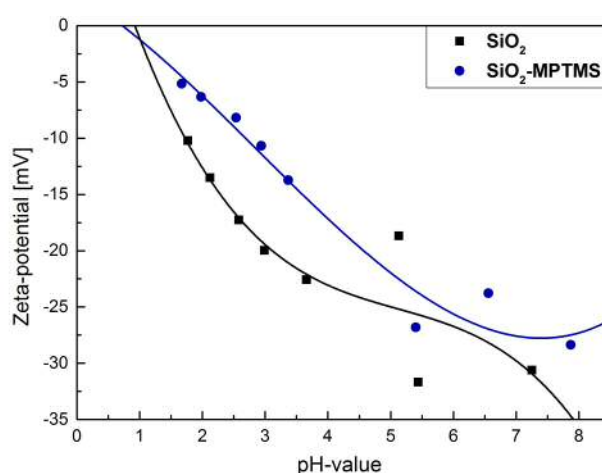


Figure 15: Zeta-potential measurements of the commercial SiO₂ nanoparticles (black) and SiO₂-MPTMS nanoparticles (blue).

The particle size was determined by dynamic light scattering, giving hydrodynamic radii of 1199 nm for the commercial SiO₂ nanoparticles, and 937 nm for SiO₂-MPTMS. The values stated by the supplier (determined via TEM) are 5-15 nm for the commercial SiO₂. Hence, the values derived from DLS measurements are indicative of agglomeration, which is less pronounced after functionalization.

4.4. Preparation of the Polymer- and Nanocomposite-based Specimens

After characterization of the functionalized nanoparticles, the nanocomposites based on the three different polymers were prepared.

4.4.1. Preparation of Nanocomposites Based on DGEBA

For the manufacturing of the nanocomposites based on DGEBA, three different cases have to be discussed:

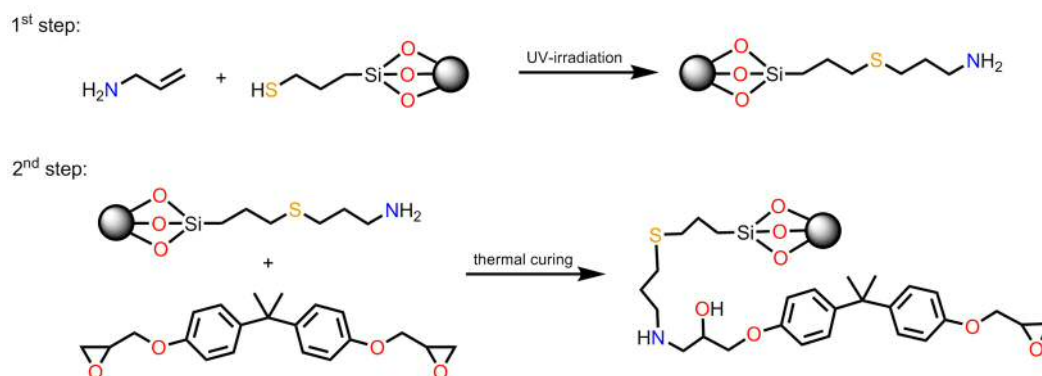
- unfilled DGEBA cured with DETA (Epoxy Resin 1),
- DGEBA cured with DETA, filled with 5 wt.-% of SiO₂ (Epoxy Resin 2),
- DGEBA cured with DETA and 5 wt.-% of SiO₂-MPTMS (Epoxy Resin 3).

Epoxy Resin 1 was prepared by mixing DGEBA with DETA and subsequent thermal curing at 90 °C, giving a transparent rigid test specimen (Figure 16). In the case of Epoxy Resin 2, the commercial SiO₂ nanoparticles were dispersed in DGEBA prior to the addition of the curing agent. As for Epoxy Resin 1, Epoxy Resin 2 was also cured at 90 °C, giving white-colored opaque test specimens (Figure 16). For Epoxy Resin 3, the SiO₂-MPTMS nanoparticles were dispersed in DGEBA. For the covalent embedment of the nanoparticles, allylamine and the photoinitiator TPO-L were added to the dispersion. For the crosslinking reaction, DETA was added. The reaction mixture was first irradiated with UV-light and then cured at 90°C. The composites of Epoxy Resin 3 showed an orange color and were opaque (Figure 16).



Figure 16: Photography of test specimen of the different epoxy resins. Left: Epoxy Resin 1, middle: Epoxy Resin 2, right: Epoxy Resin 3. The diameter of the specimens is $d = 50$ mm.

As already mentioned, for the covalent embedment of the SiO₂-MPTMS nanoparticles, allylamine was used as a linker between the epoxy-groups of DGEBA and the thiol-functionality of the SiO₂-MPTMS nanoparticles (Scheme 12). The double bond of allylamine and the thiol-group of the nanoparticle can perform thiol-ene click reaction upon irradiation with UV light. Subsequently, the amine-groups can react with the epoxy-groups of DGEBA during the thermal curing step. With this strategy, covalent bonds can be introduced between the polymer matrix and the SiO₂-MPTMS nanoparticles.



Scheme 14: Covalent embedment of the SiO₂-MPTMS nanoparticles in the DGEBA-based polymer matrix.

4.4.2. Preparation of Nanocomposites Based on Di⁻Siloxane

As for the nanocomposites based on DGEBA, also for the compounds based on Di⁻Siloxane three different cases have to be discussed:

- unfilled Di⁻Siloxane cured by the thiol-ene click reaction (Polysiloxane 1),
- Di⁻Siloxane cured via the thiol-ene click reaction and filled with 5 wt.-% of SiO₂ (Polysiloxane 2), and
- Di⁻Siloxane cured via the thiol-ene click reaction involving 5 wt.-% of SiO₂-MPTMS (Polysiloxane 3).

Polysiloxane 1 was prepared by mixing Di⁻Siloxane with 2,2'-(ethylenedioxy)-diethanethiol and trimethylolpropane-tris(3-mercaptopropionate). After addition of the photoinitiator TPO-L, vigorous stirring and subsequent irradiation with UV-light,

yellow transparent test specimens were obtained (Figure 17). In case of Polysiloxane 2 and Polysiloxane 3, the corresponding nanoparticles were dispersed in the reaction mixture prior to the addition of the photoinitiator. Both nanocomposites were obtained by irradiation with UV light as yellow and opaque test specimens (Figure 17).

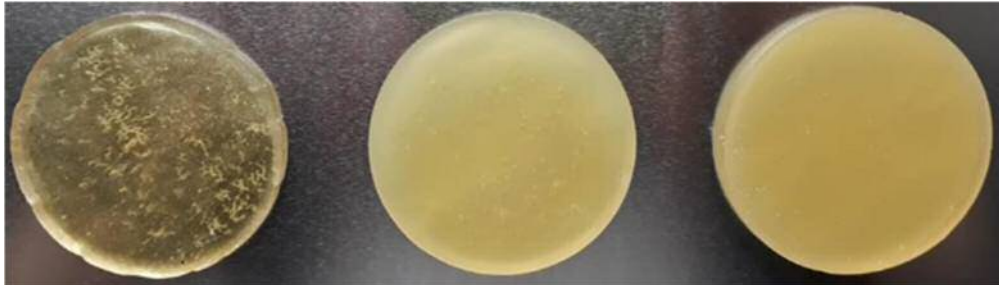
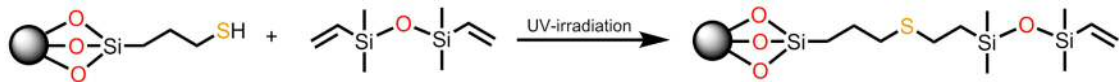


Figure 17: Test specimen of the different polysiloxanes. Left: Polysiloxane 1, middle: Polysiloxane 2, right: Polysiloxane 3. The diameter of the specimens is $d = 50$ mm.

The SiO_2 -MPTMS nanoparticles can be covalently embedded by the thiol-ene click reaction (Scheme 13). The double bonds of Di⁼Siloxane react with the thiol functionalities on the nanoparticles' surfaces, leading to covalent bonds between the polymer matrix and the nanoparticles.



Scheme 15: Covalent Embedment of the SiO_2 -MPTMS nanoparticles in the polysiloxane-based polymer matrix.

4.4.3. Preparation of Nanocomposites based on $\text{pNonOx}_{80}\text{-stat-pDec}^{\text{=}}\text{Ox}_{20}$

Again, three different cases have to be discussed:

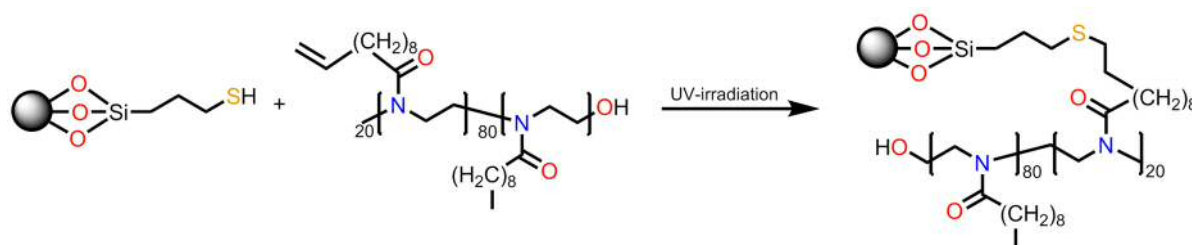
- unfilled $\text{pNonOx}_{80}\text{-stat-pDec}^{\text{=}}\text{Ox}_{20}$ cured via the thiol-ene click reaction (Polyoxazoline 1),
- $\text{pNonOx}_{80}\text{-stat-pDec}^{\text{=}}\text{Ox}_{20}$ cured by the thiol-ene click reaction and filled with 5 wt.-% of SiO_2 (Polyoxazoline 2), and
- $\text{pNonOx}_{80}\text{-stat-pDec}^{\text{=}}\text{Ox}_{20}$ cured via the thiol-ene-click reaction involving 5 wt.-% of SiO_2 -MPTMS (Polyoxazoline 3).

For Polyoxazoline 1, pNonOx₈₀-stat-pDec⁻Ox₂₀ was fine crushed in a mortar and mixed with pentaerythritol-tetra(3-mercaptopropionate) and the photoinitiator TPO-L. In case of both nanocomposites, namely Polyoxazoline 2 and Polyoxazoline 3, the nanoparticles were blended into fine crushed pNonOx₈₀-stat-pDec⁻Ox₂₀ before adding the photoinitiator. The mixed powder was platen pressed in a steel template and irradiated with UV-light, giving light-yellow test specimens (Figure 18).



Figure 18: Test specimen of the different poly(2-oxazoline)s. Left: Polyoxazoline 1, middle: Polyoxazoline 2, right: Polyoxazoline 3. The diameter of the specimens is $d = 50$ mm.

In the case of Polyoxazoline 3, the covalent embedment of the SiO₂-MPTMS nanoparticles was performed by thiol-ene click reactions (Scheme 14).



Scheme 16: Covalent Embedment of the SiO₂-MPTMS nanoparticles in the poly(2-oxazoline)-based polymer matrix.

4.5. Differential Scanning Calorimetry of the Polymers and the Nanocomposites

Aiming to check if the addition of the nanoparticles has an impact on the glass-transition temperatures, DSC measurements were performed (Table 3). It is evident that the addition of nanoparticles does not lead to any significant change in the glass-transition temperatures of the Polysiloxanes 1-3 and the Polyoxazolines 1-3. In case of the epoxy resins, the glass-transition temperature of Epoxy Resin 2 is slightly

lower than those of Epoxy Resin 1 and Epoxy Resin 3. This leads to the assumption that the commercial SiO₂ are not homogeneously distributed in the polymer matrix, leading to lower intermolecular forces.

Table 3: Glass-transition temperatures of the different polymers and nanocomposites.

Polymer or composite	Glass-transition temperature [°C]
Epoxy Resin 1	112
Epoxy Resin 2	108
Epoxy Resin 3	114
Polysiloxane 1	144
Polysiloxane 2	145
Polysiloxane 3	144
Polyoxazoline 1	144
Polyoxazoline 2	145
Polyoxazoline 3	144

4.6. Curing Kinetics of the Polymers and the Nanocomposites

Differential Scanning Calorimetry cannot only be used to quantify the influence of the nanoparticles on, for example, the glass-transition temperatures. Via DSC, also the curing kinetics of the unfilled polymers and the impact of the nanoparticles on its kinetics, including the covalent embedment of the SiO₂-MPTMS nanoparticles, could be investigated. Therefore, all samples were measured twice with three different heating rates of 5, 10, and 20 K·min⁻¹. The conversion curves were determined from the heat flow vs. sample temperature curves, using a spline baseline fit for integration. All activation energies were calculated according to Kissinger. [73]

4.6.1. Curing Kinetics of Epoxy Resins

In case of the epoxy resins, each sample revealed one peak, independent of the absence or presence of nanofillers. Concerning the shape of the heat flow vs. sample temperature curve (Figure 19), no impact of the commercial SiO₂ or SiO₂-MPTMS on the curing kinetics is observable. The same is true for the conversion curves, which are also illustrated in Figure 19.

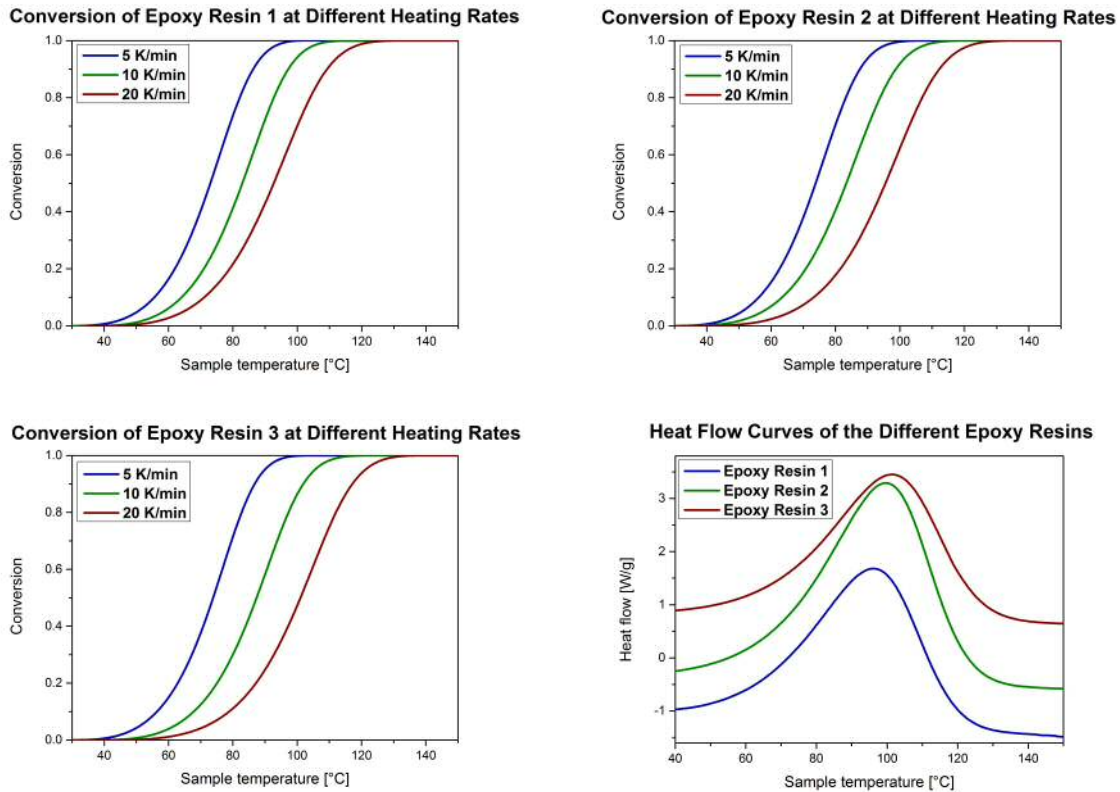


Figure 19: Heat flow vs. sample temperature curves and conversion curves of the different epoxy resins.

The conversion curves for all three epoxy resins show the same trend: With increasing heat rate, full conversion is shifted to higher temperatures. The full conversion temperatures are shifted from about 90 °C at 5 K·min⁻¹ to about 100 °C at 10 K·min⁻¹ and to about 110 °C at 20 K·min⁻¹ due to shorter ‘residence times’ at the respective elevated temperatures. It can also be seen that the conversion curve has a slight increase at the beginning of the reaction indicative of the system’s slow response at the start of the curing process. This behavior is observed for each epoxy resin. From the conversion curves, the activation energies for the different epoxy resins were calculated according to Kissinger (Table 4).

Table 4: Activation energies for the curing of the different epoxy resins according to Kissinger.

Polymer / Composite	Activation energy [kJ·mol ⁻¹]
Epoxy Resin 1	62.1
Epoxy Resin 2	57.7
Epoxy Resin 3	54.1

The highest activation energy is observed for Epoxy Resin 1 with $62.1 \text{ kJ}\cdot\text{mol}^{-1}$. Upon the addition of commercial SiO_2 nanoparticles, the activation energy is lowered. This is probably due to the hydroxy groups present on the SiO_2 surface, which can catalyze the ring-opening reaction of epoxides. The activation energy for the curing of Epoxy Resin 3 is lower than that of Epoxy Resin 2. This indicates that the covalent embedment of the nanoparticles takes place in the same temperature range as aside the curing reaction itself. Furthermore, the low value of the activation energy is probably due to the low activation energy of the covalent embedment reaction, decreasing the overall activation energy in case of Epoxy Resin 3.

4.6.2. Curing Kinetics of Polysiloxanes

In the heat flow vs. sample temperature curves of the polysiloxanes, Polysiloxane 1 and Polysiloxane 2 show both one peak only. With the addition of the SiO_2 -MPTMS nanoparticles, the shape of the heat flow vs. temperature curve changes: An additional peak can be identified at lower sample temperatures than the curing reaction (Figure 20). The same trend is observable for the conversion curves, which are shown in Figure 21.

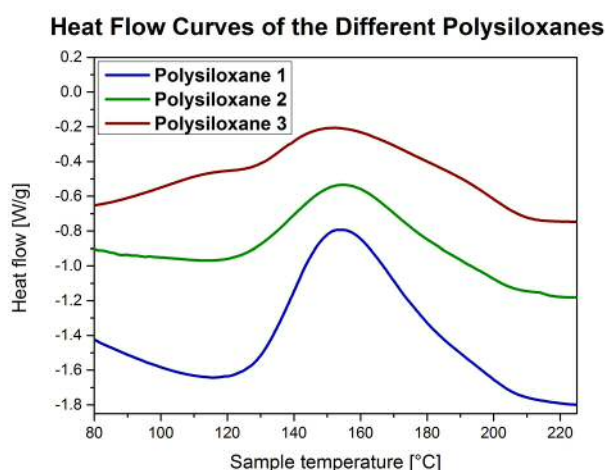


Figure 20: Heat flow vs. sample temperature curves of the different polysiloxanes.

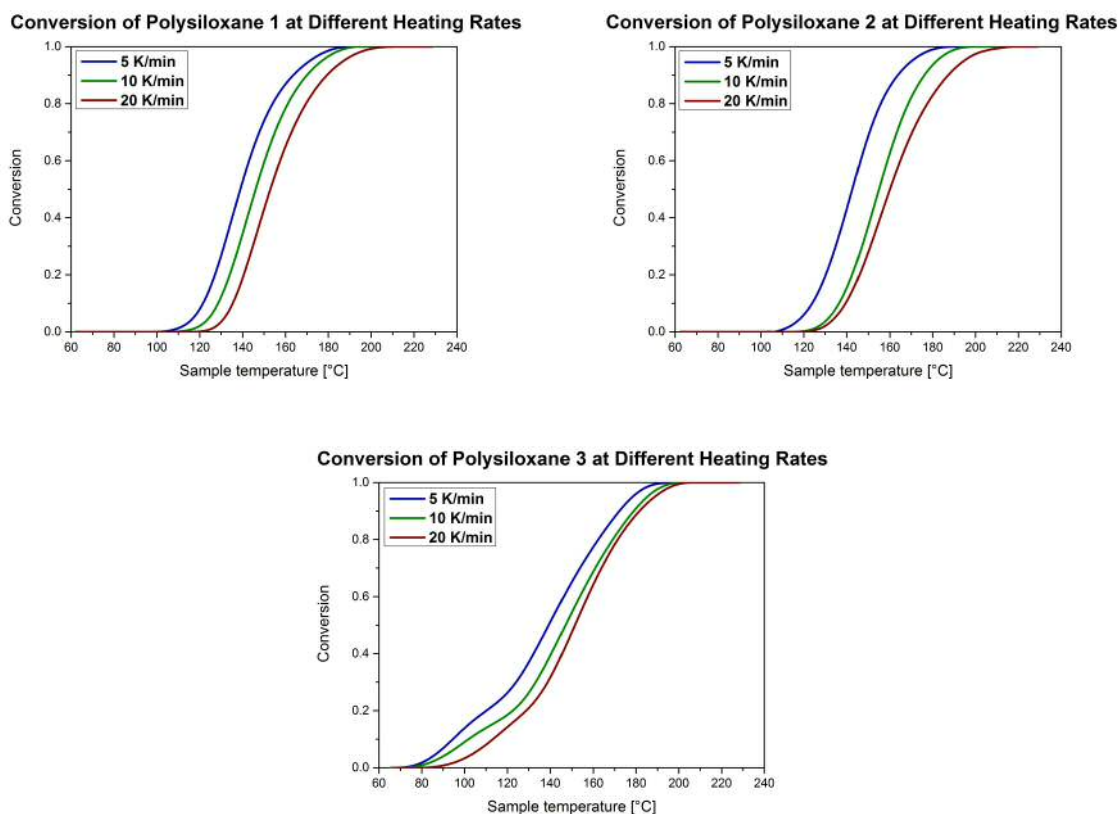


Figure 21: Conversion curves of the different polysiloxanes at different heating rates.

A pronounced shape of the conversion curve in the low-temperature region is observable for Polysiloxane 3. This is presumably due to the fact that the covalent embedment of the SiO₂-MPTMS nanoparticles takes place before the curing reaction starts, leading to an initial increase of the slope until the maximum of the covalent embedment reaction is reached. Afterwards, the slope of the conversion curve is decreased again, before it increases again due to the start of the curing reaction. Similarly, as it was shown for the epoxy resins, also the polysiloxanes show the same trend: With increasing heating rate, the full conversion is shifted to higher temperatures.

From the conversion curves, the activation energies for the curing of the different polysiloxanes were calculated according to Kissinger (Table 5). In case of Polysiloxane 1, the activation energy is as high as 154.9 kJ·mol⁻¹; this value is lower in the cases of Polysiloxane 2-3. As no catalytic effect of the hydroxy groups present on the SiO₂ nanoparticles surface can be argued for this crosslinking reaction, this

investigation will be continued at a later stage in order to retrace this phenomenon to the molecular level. Notably and unambiguously, the activation energy of the covalent embedment of the SiO₂-MPTMS nanoparticles in the case of Polysiloxane 3 shows a comparably low value.

Table 5: Activation energies for the curing of the different polysiloxanes according to Kissinger.

Polymer / Nanocomposite	Activation energy [kJ·mol ⁻¹]	
	Curing reaction	Covalent embedment
Polysiloxane 1	154.9	
Polysiloxane 2	131.2	
Polysiloxane 3	119.3	56.1

4.6.3. Curing Kinetics of Poly(2-oxazoline)s

In case of the poly(2-oxazoline)s, each sample revealed one peak of the heat flow vs. sample temperature curves (Figure 22). No difference concerning Polyoxazoline 1 and Polyoxazoline 2 can be noticed in the shape of the heat flow vs. sample temperature curve. With the addition of SiO₂-MPTMS nanoparticles, the shape of the heat flow vs. temperature curve changes: An additional peak can be identified at lower sample temperatures than the curing reaction in the case of Polyoxazoline 3 (Figure 22). The same is true for the conversion curves (Figure 23).

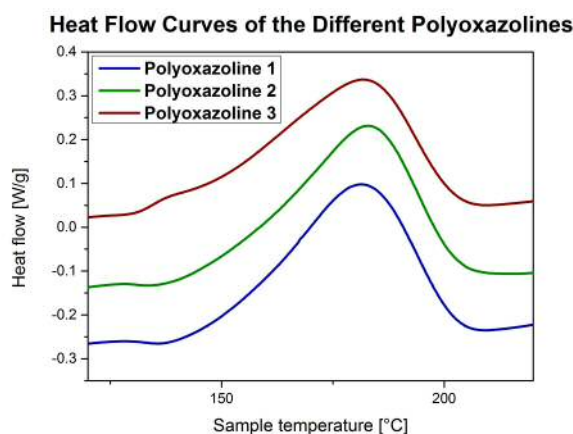


Figure 22: Heat flow vs. sample temperature curves of the different poly(2-oxazoline)s.

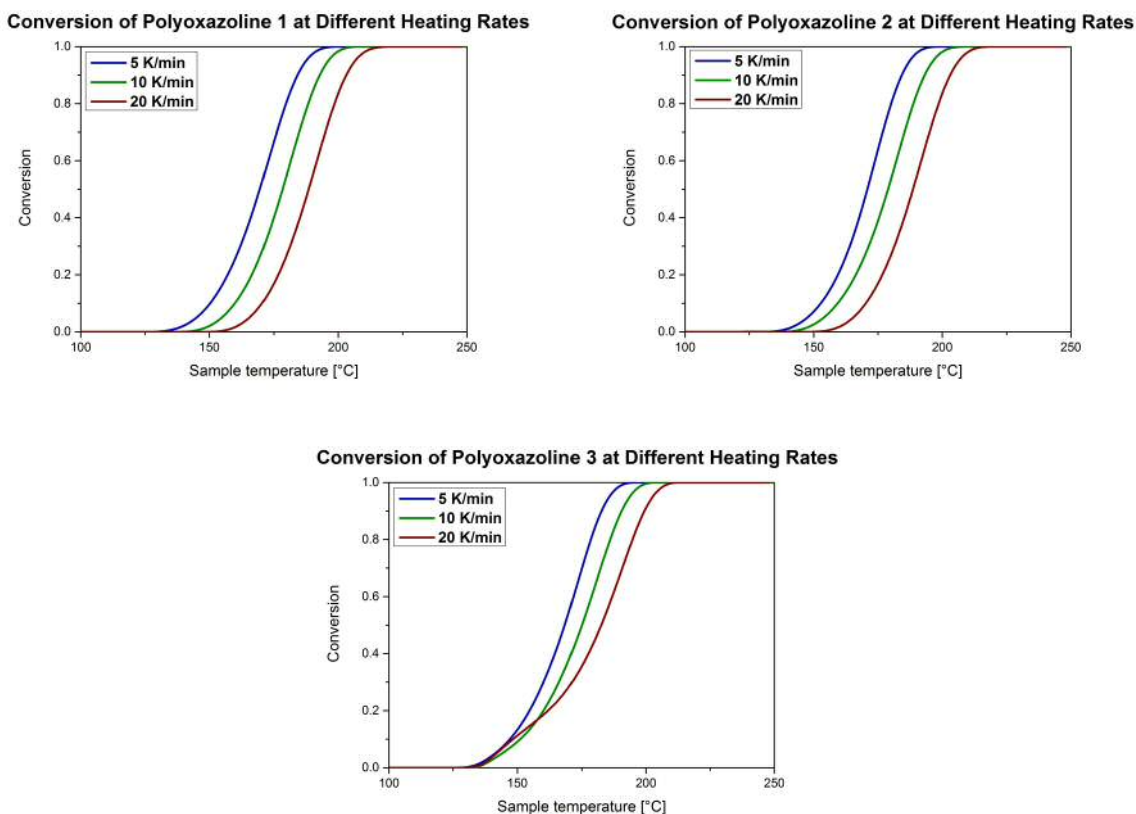


Figure 23: Conversion curves of the different poly(2-oxazoline)s at different heating rates.

The conversion curves for Polyoxazoline 1 and Polyoxazoline 2 are similar with 100% conversion at temperatures of around 195 °C at 5 K·min⁻¹, around 200 °C at 10 K·min⁻¹ and around 205 °C at 20 K·min⁻¹. These temperatures are also valid for Polyoxazoline 3, but the shape at the beginning of the curve differs from the other two. As already observed at the polysiloxanes, the covalent embedment reaction of the SiO₂-MPTMS nanoparticles takes place before the curing reaction starts, leading to differences due to changes concerning the slope.

From the conversion curves, the activation energies for the curing of the different poly(2-oxazoline) resins were calculated according to Kissinger (Table 6). In case of the poly(2-oxazoline)s, all activation energies, including the one for covalent embedment, are quite similar ranging from 119.2 to 128.6 kJ·mol⁻¹.

Table 6: Activation energies for the curing of the different poly(2-oxazoline)s according to Kissinger.

Polymer / Nanocomposite	Activation energy [kJ·mol ⁻¹]	
	curing reaction	covalent embedment
Polyoxazoline 1	119.24	
Polyoxazoline 2	121.08	
Polyoxazoline 3	126.66	128.59

4.7. Transmission Electron Microscopy of the Polymers and the Nanocomposites

In addition to the investigation of the curing processes with DSC, TEM measurements were performed in order to determine if the covalent embedment of nanoparticles leads to less agglomeration in the polymer matrix.

4.7.1. TEM Measurements of the Epoxy Resins

TEM pictures of the Epoxy Resin 1-3 at a magnification of 6500 (Figure 24) reveal that the commercial SiO₂ nanoparticles (in case of Epoxy Resin 2) show a higher tendency to agglomerate in the polymer matrix than their functionalized analogues (in case of Epoxy Resin 3).

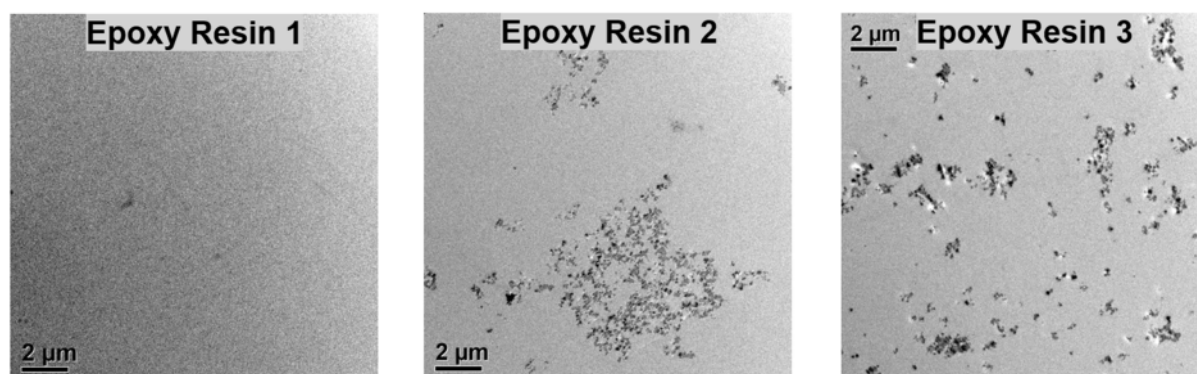


Figure 24: TEM pictures of Epoxy Resin 1-3 at a magnification of 6,500.

Hence, in Epoxy Resin 3, the SiO₂-MPTMS nanoparticles seem to be much more homogeneously distributed in the polymer matrix than the non-functionalized SiO₂ nanoparticles in Epoxy Resin 2. This trend is also verified when looking at higher magnitudes (Figure 25).

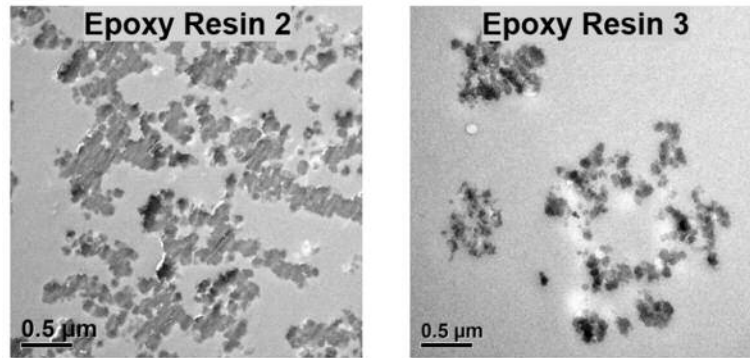


Figure 25: TEM pictures of Epoxy Resin 2-3 at a magnification of 30,000.

At high magnification images, it is evident that the SiO₂-MPTMS nanoparticles seem to have ‘softer edges’ compared to the commercial SiO₂ nanoparticles. Moreover, in some regions, the SiO₂-MPTMS nanoparticles look like they are surrounded by white shields. At a magnification of 67,000, these shields can be clearly seen (Figure 26). These shields that surround the SiO₂-MPTMS nanoparticles can be due to some unreacted educts (allylamine, DETA) or localized phase separation of the nanoparticles’ MPTMS shell and the polymer matrix. Unremoved functionalization agent can be excluded as such shields cannot be found in the other nanocomposites, while the same batch of SiO₂-MPTMS was used for all nanocomposites.

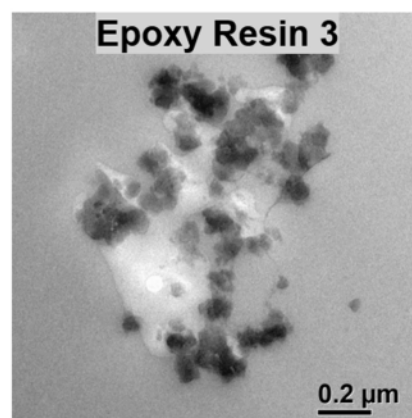


Figure 26: TEM picture of Epoxy Resin 3 at a magnification of 67,000.

4.7.2. TEM Measurements of the Polysiloxanes

In Polysiloxane 2, to which commercial SiO₂ nanoparticles were added, a similar tendency to agglomeration as in Epoxy Resin 2 can be observed (Figure 27). In case of Polysiloxane 3, the SiO₂-MPTMS nanoparticles seem to be more homogeneously distributed.

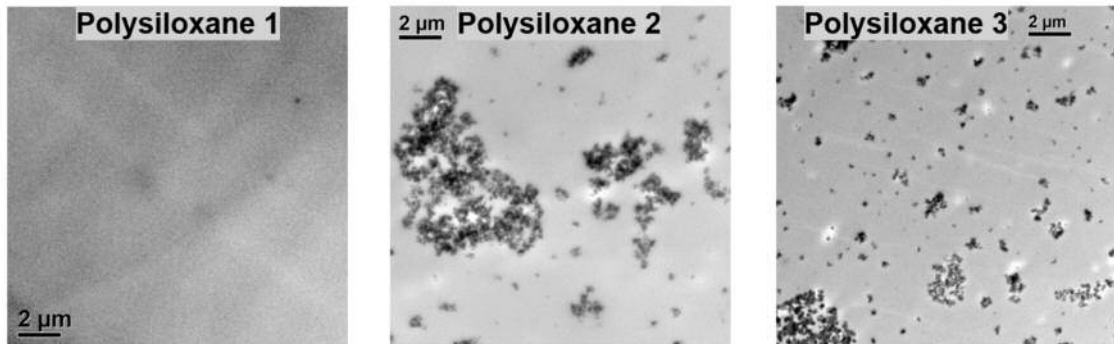


Figure 27: TEM pictures of the Polysiloxanes 1-3 at a magnification of 6,500.

This trend is also observed at higher magnitudes (Figure 28). In case of Polysiloxane 2, only two big agglomerates are depicted at a magnification of 30,000, whereas for Polysiloxane 3 much smaller agglomerates can be observed.

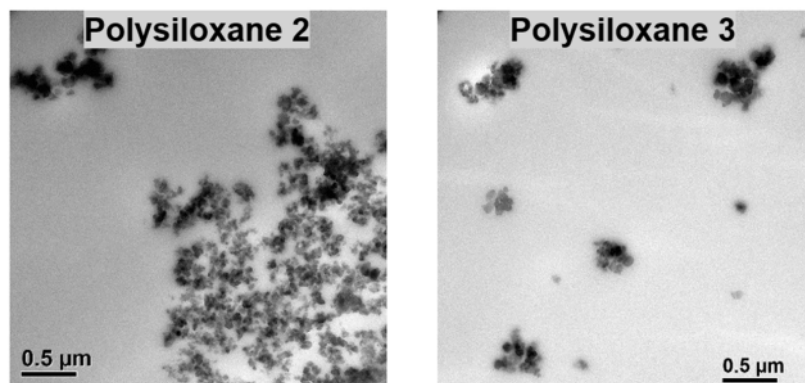


Figure 28: TEM pictures of the Polysiloxanes 2-3 at a magnification of 30,000.

Overall, the assumption that the covalent embedment of nanoparticles in a polymer matrix could lead to decreasing agglomeration was verified for the polysiloxanes as well.

4.7.3. TEM Measurements of the Poly(2-oxazoline)s

The TEM images of Polyoxazoline 1-3 (Figure 29) reveal again that, upon the addition of commercial SiO₂ in Polyoxazoline 2, agglomeration of the commercial nanoparticles can be observed, as already described for Epoxy Resin 2 and Polysiloxane 2. This trend is significantly less observable for the functionalized nanoparticles in Polyoxazoline 2.

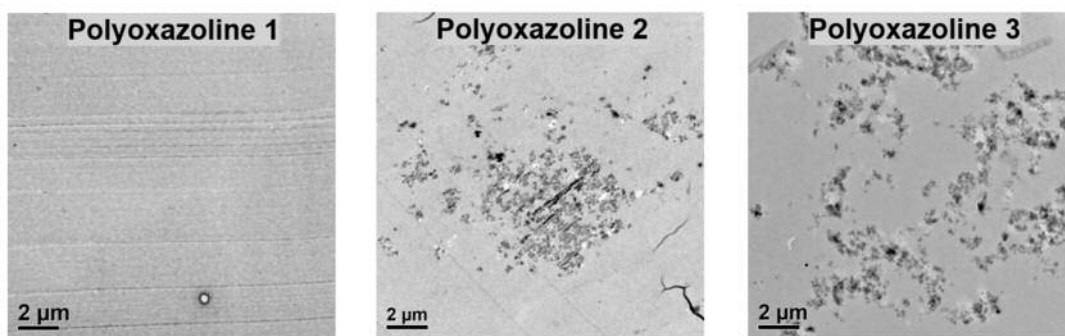


Figure 29: TEM pictures of the Polyoxazolines 1-3 at a magnification of 6,500.

The same trend is identified at higher magnifications (Figure 30). While admittedly also the SiO₂-MPTMS nanoparticles show a tendency to agglomerate, it is lower than that of the commercial SiO₂ nanoparticles. In comparison with Epoxy Resin 3 or Polysiloxane 3, agglomeration cannot be avoided in pNonOx₈₀-*stat*-pDec⁻Ox₂₀ with this strategy to the same extent as it was possible for the other polymer systems.

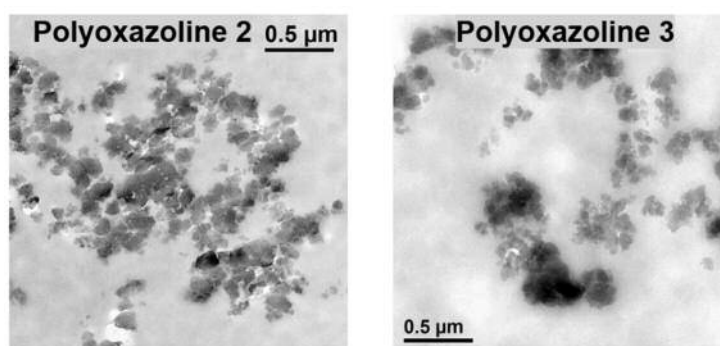


Figure 30: TEM pictures of the Polyoxazolines 2-3 at a magnification of 30,000.

The agglomeration of the functionalized nanoparticles could be due to the long side-chains in pNonOx₈₀-*stat*-pDec⁻Ox₂₀. In fact, the NonOx side chains are known to have a favored structural orientation towards the surface which consequently exhibits

nano-roughness ('hydrophobic recovery'), [74] which can be also observed with TEM measurement within this study (Figure 31). It can be assumed that due to this favored structural orientation, the SiO₂-MPTMS nanoparticles' tendency to agglomerate is more promoted than in the other two polymer systems.

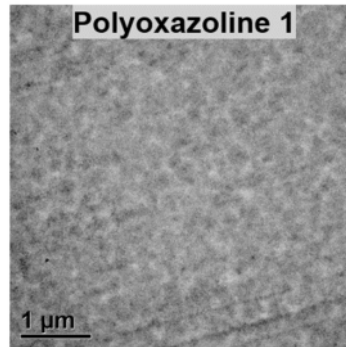


Figure 31: TEM pictures of Polyoxazoline 1 at a magnification of 21,000.

4.8. Thermal Conductivity of the Polymers and the Nanocomposites

For further characterization of the nanocomposites, the thermal conductivity of all nine samples was determined. Therefore, test specimens with a diameter of 50 mm and a height of 2 mm were analyzed at 30, 60, and 90 °C. For every nanocomposite, double determination at all three temperatures was performed. For further discussion, only the average values are used.

4.8.1. Thermal Conductivity of the Epoxy Resins

In case of the epoxy resins, the thermal conductivity ranges from 0.12 to 0.16 W·m⁻¹·K⁻¹ at 30 °C, from 0.13 to 0.17 W·m⁻¹·K⁻¹ at 60 °C, and from 0.16 to 0.19 W·m⁻¹·K⁻¹ at 90 °C (Figure 32). Hence, as expected, the thermal conductivity increases with increasing temperature. This is due to the advancement near the glass-transition temperature, which is around 110 °C for all epoxy resins. No significant change of thermal conductivity can be observed upon the addition of commercial SiO₂ or SiO₂-MPTMS.

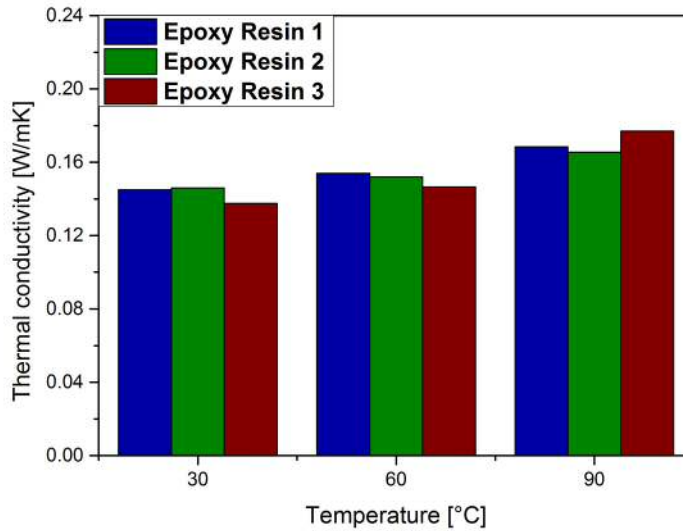


Figure 32: Thermal conductivity of Epoxy Resin 1-3 at temperatures of 30, 60, and 90 °C.

4.8.2. Thermal Conductivity of Polysiloxanes

For the polysiloxanes, it can be clearly seen that the thermal conductivity is the highest for Polysiloxane 1, into which no nanoparticles are added (Figure 33). The values for Polysiloxane 1 range between 0.10 and $0.12 \text{ W}\cdot\text{m}^{-1}\cdot\text{K}^{-1}$ and do not increase with increasing temperature as it was observed for the epoxy resins. This could be due to the fact that the polysiloxanes have a higher glass-transition point around $140 \text{ }^\circ\text{C}$. In comparison, the values for Polysiloxane 2 and Polysiloxane 3 are lower with 0.8 to $0.9 \text{ W}\cdot\text{m}^{-1}\cdot\text{K}^{-1}$. As already observed for the epoxy resins, no impact of the covalent embedment on the thermal conductivity is observable.

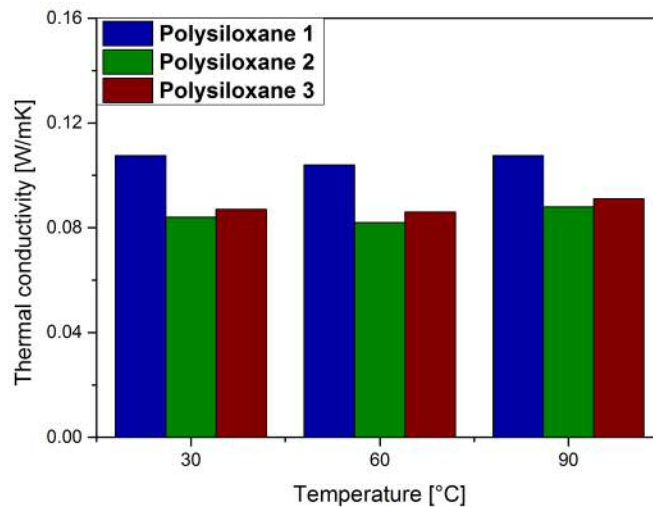


Figure 33: Thermal conductivity of Polysiloxane 1-3 at temperatures of 30, 60, and 90 °C.

4.8.3. Thermal Conductivity of the Poly(2-oxazoline)s

The values of the thermal conductivity range from 0.11 to 0.13 $\text{W}\cdot\text{m}^{-1}\cdot\text{K}^{-1}$ for Polyoxazoline 1, from 0.12 to 0.16 $\text{W}\cdot\text{m}^{-1}\cdot\text{K}^{-1}$ for Polyoxazoline 2, and from 0.13 to 0.17 $\text{W}\cdot\text{m}^{-1}\cdot\text{K}^{-1}$ for Polyoxazoline 3 (Figure 34). In comparison to Epoxy Resin 1-3 and Polysiloxane 1-3, the thermal conductivity of the poly(2-oxazoline)s slightly increases upon the addition of the nanoparticles. This is the case for both nanoparticles, the commercial SiO_2 nanoparticles and the SiO_2 -MPTMS ones; the SiO_2 -MPTMS particles enable higher thermal conductivity than the commercial non-functionalized ones.

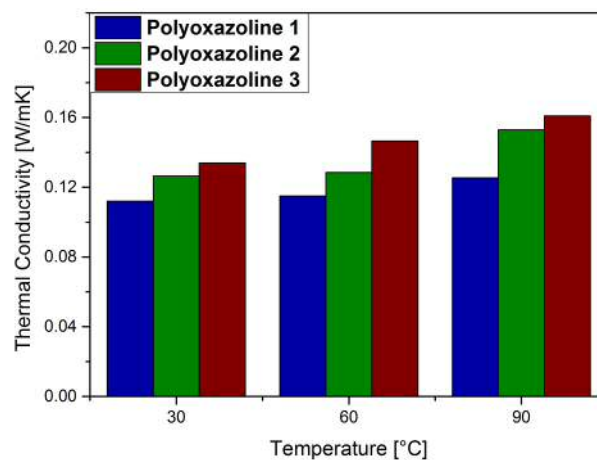


Figure 34: Thermal conductivity of Polyoxazoline 1-3 at temperatures of 30, 60, and 90 °C.

4.9. Water Uptake of the Polymers and the Nanocomposites

Aside from the thermal conductivity, also the water uptake is an important characteristic for nanodielectrics. In this study, water uptake was quantified for the different nanocomposites over a timeframe of 30 d in a climate chamber at 30 °C and humidity of 85%. The water uptake was quantified gravimetrically; double determination was performed in every case. For further discussion, the mean values are used.

4.9.1. Water Uptake of the Epoxy Resins

The time-dependent water uptake of Epoxy Resin 1-3 (Figure 35) shows the expected approach towards maximum values, which amount to 1.5 wt.-% for Epoxy Resin 1 and Epoxy Resin 3, and 1.3 wt.-% for Epoxy Resin 2. For all three epoxy resins, the equilibrium is reached after 4 weeks. Interestingly, the water uptake of Epoxy Resin 1 and Epoxy Resin 3 is similar, indicating that due to the covalent embedment and better distribution of the nanoparticles, the water uptake is more similar to the unfilled polymer than to the one filled with commercial SiO₂. Notably, the water uptake of Epoxy Resin 2 is lower than that of Epoxy Resin 1 and Epoxy Resin 3.

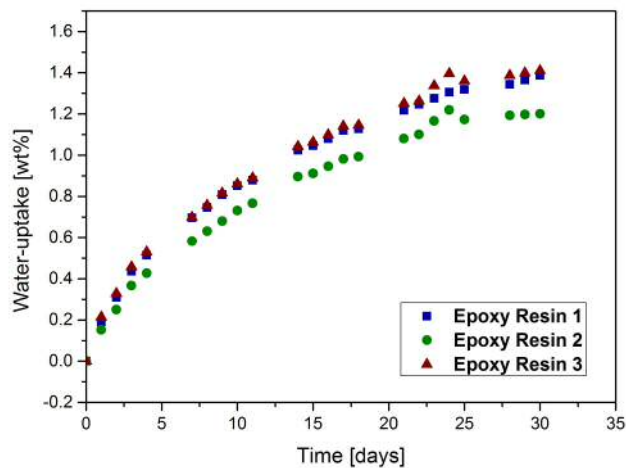


Figure 35: Water uptake of Epoxy Resins 1-3 at a temperature of 30 °C and a humidity of 85%.

4.9.2. Water Uptake of the Polysiloxanes

The water uptake of Polysiloxane 1-3 is much lower than that of the epoxy resins (Figure 36). This is due to the more hydrophobic, non-polar character of the polymer matrix of the polysiloxanes. For Polysiloxane 1, the maximum water uptake is about 0.5 wt.-%; for Polysiloxane 3, it is about 0.6 wt.-%. As observed for the epoxy resins, the unfilled polymer and the one with covalently embedded nanoparticles show similar behavior. Analogously, Polysiloxane 2, which is filled with commercial SiO₂ nanoparticles, shows a water uptake of only 0.3 wt.-%. This indicates again that the much more homogenous distribution of the nanoparticles in the polymer matrix leads to a water uptake more comparable with the one of the unfilled polymers. A

difference to the epoxy resins is the fact that the equilibrium is reached really fast for Polysiloxane 2 within only one week. For Polysiloxane 1/ 3, the equilibrium was reached after 4 weeks like for the epoxy resins. The water uptake of Polysiloxane 1 and Polysiloxane 3 is nearly double that high as for Polysiloxane 2, which was not observable in case of the epoxy resins, where the difference in water uptake was only about 10 %.

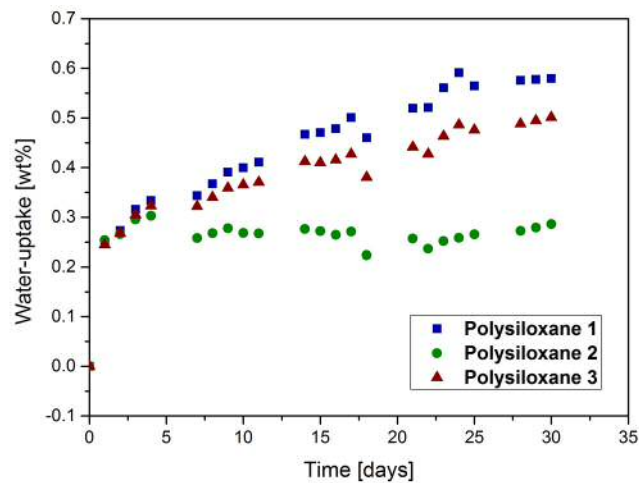


Figure 36: Water uptake of Polysiloxane 1-3 at a temperature of 30 °C and a humidity of 85%.

4.9.3. Water Uptake of the Poly(2-oxazoline)s

The process of water uptake is much faster for the poly(2-oxazoline)s than for the other two polymers (Figure 37). In all cases, the water uptake reaches an equilibrium after only one week. As for the epoxy resins and the polysiloxanes, the water uptake is the highest for the unfilled polymer with about 1.7 wt.-%. Differently from the behavior of the epoxy resins and the polysiloxanes, the water uptake for both filled polymers, Polyoxazoline 2 and Polyoxazoline 3, is similar with 1.5 wt.-%. Since the distribution of the nanoparticles was not as homogenous as for the epoxy resins and the polysiloxanes, it can be assumed that the water uptake is similar for both filled poly(2-oxazoline)s due to the similar agglomeration of the nanoparticles in the polymer matrix.

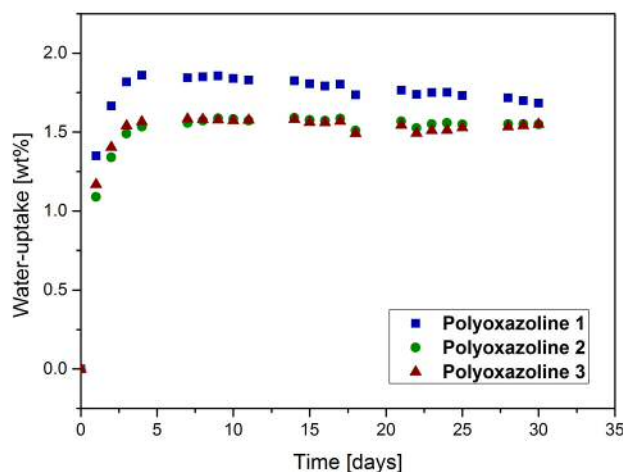


Figure 37: Water uptake of Polyoxazolines 1-3 at a temperature of 30 °C and a humidity of 85%.

4.10. Dielectric Characterization of the Polymers and the Nanocomposites

Also the dielectric characterization of all nine nanocomposites was performed. Therefore, square foils were prepared, and the permittivity and dielectric loss were recorded in a frequency range from 1 mHz to 5 kHz. Every nanocomposite was measured after drying for three d at 90 °C in the drying oven (hereinafter referred to as, e.g., dry Epoxy Resin 1) and after storage in the climate chamber for 3 weeks (hereinafter referred to as, e.g., wet Epoxy Resin 1). Prior to the measurements, also the measuring cell, including the electrodes, was dried in the drying oven. In every case, double determination of the parameters was performed. For further discussion, the averaged values are taken into concern.

4.10.1. Dielectric Characterization of the Epoxy Resins

For Epoxy Resin 1-3, the permittivity (real part, as well as imaginary part) increases with decreasing frequencies (Figure 38). Interestingly, the real part of the permittivity of Epoxy Resin 2 resembles that of Epoxy Resin 1 for low frequencies and that of Epoxy Resin 3 for high frequencies. Hence, while Epoxy Resin 1 and Epoxy Resin 3 favorably only show slight changes of the real part of the permittivity (from 4.2 to 4.4 and from 3.3 to 3.7, respectively), Epoxy Resin 2 shows pronounced changes from 3.3 to 4.3.

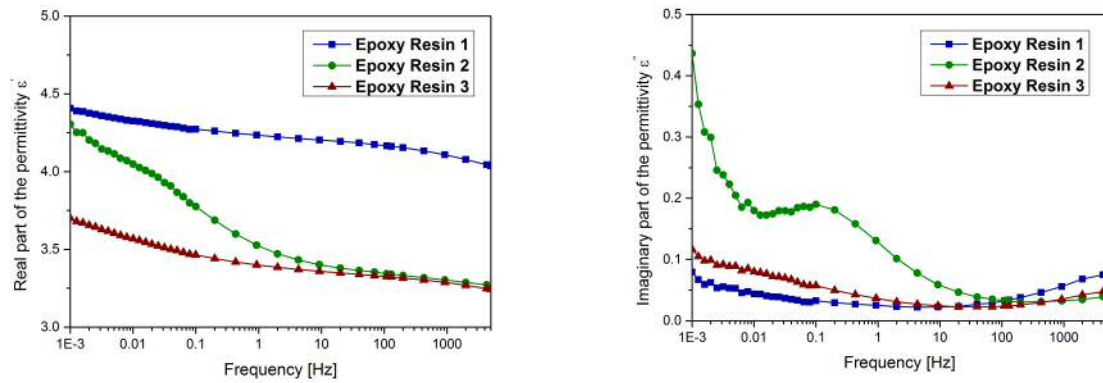


Figure 38: Real part of the permittivity (left) and imaginary part of the permittivity (right) of the different epoxy resins.

At frequencies below 1 Hz, the permittivity of Epoxy Resin 2 increases due to interfacial polarization in the boundaries between the polymer matrix and the commercial SiO_2 nanoparticles that bear a plethora of OH functionalities. Furthermore, due to the high number of hydroxy groups present on the commercial SiO_2 surfaces, also dipole-dipole interactions cannot be neglected. By contrast, this increase of the real part of the permittivity is not observable for Epoxy Resin 3. It is evident that, due to the covalent embedment and surface functionalization of the nanoparticles, the interfacial polarization in the boundaries between the polymer and nanoparticles interface can be prevented. In fact, the shape of the curve for the real part of the permittivity of Epoxy Resin 3 is similar to the one of Epoxy Resin 1 – in both cases, only a slight increase over the frequency range was determined. The trend observable for the real part of the permittivity is also noticed for the imaginary part: Epoxy Resin 2 shows a high increase of the imaginary part of the permittivity at low frequencies, whereas this increase cannot be observed for Epoxy Resin 1 and Epoxy Resin 3.

At 20 °C and 40 Hz (Table 7), Epoxy Resin 1 shows a real part of the permittivity of 4.19. The value of 3.37 for Epoxy Resin 2 is lower, which fits with literature data. [14] The value of 3.34 of Epoxy Resin 3 is similar to that of Epoxy Resin 2.

Table 7: Real and imaginary part of the permittivity of the different epoxy resins at 40 Hz and 20 °C.

Polymer / Nanocomposite	ϵ'	ϵ''
Epoxy Resin 1	4.19	0.027
Epoxy Resin 2	3.37	0.039
Epoxy Resin 3	3.34	0.023

Apart from permittivity, also the dielectric loss was determined, for the wet as well as the dry epoxy resins (Figure 39). Similar to the permittivity, the dielectric loss increases with decreasing frequencies. This is true for dry Epoxy Resin 1, dry Epoxy Resin 3, and all wet epoxy resins. In the case of dry Epoxy Resin 2, a more complex behavior can be observed: A local maximum is reached at 0.5 Hz; the dielectric loss increases again for frequencies lower than 10 mHz, notably to a much larger extent than in the case of dry Epoxy Resin 1 or dry Epoxy Resin 3. The dielectric loss is highly affected from water present in the material. As already described earlier, commercial SiO₂ has a high amount of water adsorbed on its surface. These adsorbed water molecules are assumed to lead to the observed curve shape of dry/wet Epoxy Resin 2.

For good dielectrics, the dielectric loss has to be $\tan\delta \ll 1$. This criterion is fulfilled for all dry epoxy resins in the frequency range from 1 mHz to 5 kHz. In case of the wet epoxy resins, only Epoxy Resin 1 and Epoxy Resin 3 maintain insulating properties at the lower frequencies. Epoxy Resin 2 loses its insulating properties starting from frequencies lower than 10 mHz, and afterwards the dielectric loss increases very quick.

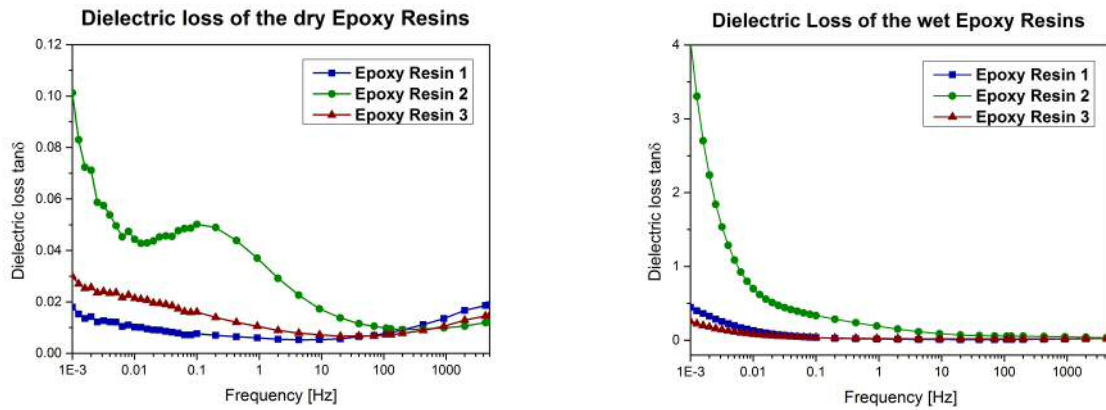


Figure 39: Dielectric loss of the dry (left) and wet (right) epoxy resins.

Dielectric losses, as well as the ratio of wet to dry, of the epoxy resins are summarized in Table 8. The lowest increase of dielectric loss is observed for Epoxy Resin 1, with a value of only 1.40. The ratio of Epoxy Resin 2 has a higher value of 5.47. The difference is due to the hydroxy groups present on the commercial SiO₂ surface. With the covalent embedment of the functional particles in Epoxy Resin 3, the ratio between dry and wet can be decreased a lot.

Table 8: Dielectric Loss of the different epoxy resins at 40 Hz and 20 °C.

Polymer / Nanocomposite	$\tan\delta_{\text{dry}}$	$\tan\delta_{\text{wet}}$	$\tan\delta_{\text{wet}} : \tan\delta_{\text{dry}}$
Epoxy Resin 1	0.0065	0.0091	1.40
Epoxy Resin 2	0.0115	0.0629	5.47
Epoxy Resin 3	0.0068	0.0198	2.91

4.10.2 .Dielectric Characterization of the Polysiloxanes

The permittivity (real part, as well as imaginary part) increases with decreasing frequencies for all polysiloxanes (Figure 40). Notably (cp. hereinabove), at low frequencies, Polysiloxane 2 mimics Polysiloxane 1, while at high frequencies, it behaves very similar to Polysiloxane 3. At frequencies lower than 10 Hz, the following trends can be observed: The permittivity of Polysiloxane 1 and Polysiloxane 2 start to increase due to dipole-dipole interactions in the polymer matrix. In case of

Polysiloxane 3, the increase that is also due to interfacial polarization occurs to lower extent.

Concerning the imaginary part of the permittivity, Polysiloxane 1 and Polysiloxane 3 show a higher increase compared to Polysiloxane 2. However, the imaginary parts of all three polysiloxanes show increase at lowered frequencies.

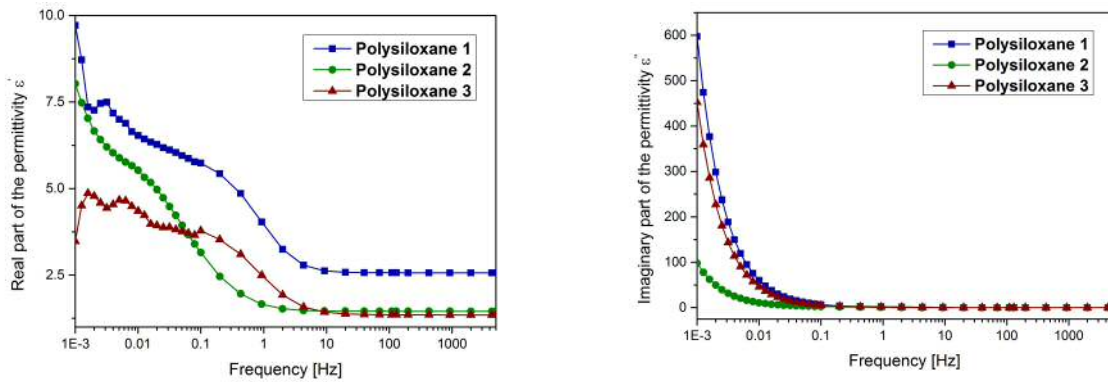


Figure 40: Real part of the permittivity (left) and imaginary part of the permittivity (right) of the different polysiloxanes.

The real and the imaginary part of the permittivity for all three polysiloxanes are summarized in Table 9.

Table 9: Real and imaginary part of the permittivity of the different polysiloxanes at 40 Hz and 20 °C

Polymer / Nanocomposite	ϵ'	ϵ''
Polysiloxane 1	2.57	0.098
Polysiloxane 2	1.46	0.020
Polysiloxane 3	1.36	0.091

The value of the real part of the permittivity for Polysiloxane 1 is 2.569; the value of around 1.4 of Polysiloxane 2/3 is lower. Hence, it can be assumed that the decrease of the real part of the permittivity is due to the addition of silica nanoparticles.

Apart from the permittivity, also the loss factor was determined (Figure 41). Similar to the permittivity, the dielectric loss increases with decreasing frequencies. In case of the dry polysiloxanes, the same trend as observed for the imaginary part of the permittivity is observed: Polysiloxane 1 and Polysiloxane 3 show higher increase than Polysiloxane 2. Since the dielectric loss is highly affected by water present in the material, the dielectric loss of all types of wet polysiloxanes are very similar.

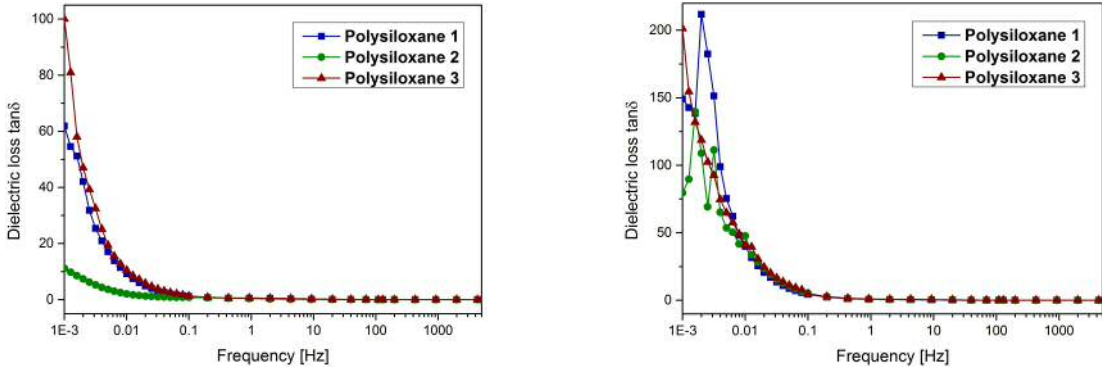


Figure 41: Dielectric loss of the dry (left) and wet (right) polysiloxanes.

A comparably low increase of the dielectric loss (dry/wet) can be observed for Polysiloxane 1/3 (Table 10; value of 2.92). The ratio in the case of Polysiloxane 2 of 13.76 is significantly higher.

Table 10: Dielectric loss of the different polysiloxanes at 40 Hz and 20 °C.

Polymer / Nanocomposite	$\tan\delta_{dry}$	$\tan\delta_{wet}$	$\tan\delta_{wet} : \tan\delta_{dry}$
Polysiloxane 1	0.0381	0.1114	2.92
Polysiloxane 2	0.0142	0.1953	13.76
Polysiloxane 3	0.0663	0.1937	2.92

4.10.3. Dielectric Characterization of the Poly(2-oxazoline)s

For the poly(2-oxazoline)s, the permittivity (real part, as well as imaginary part) increases with decreasing frequencies as well (Figure 42). Unlike the epoxy resins and the polysiloxanes, Polyoxazoline 3 behaves more similar to Polyoxazolin 2 in the region of low frequencies: At frequencies below 0.1, the increase of the real and the imaginary part of the permittivity is highest for Polyoxazoline 1, followed by Polyoxazoline 3 and Polyoxazoline 2. In case of the poly(2-oxazoline)s, the interfacial polarization in the polymer chain seems higher than the one between the nanoparticles and the polymer matrix. Furthermore, with the addition of the nanofillers, the polarizability of the polymer matrix seems lowered.

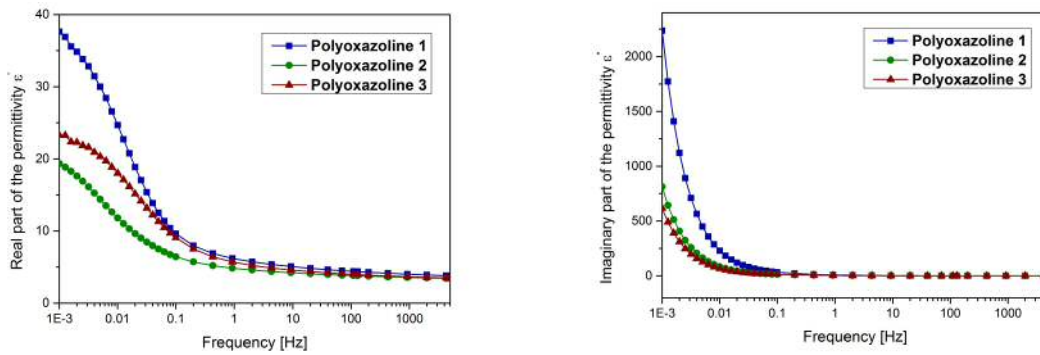


Figure 42: Real part of the permittivity (left) and imaginary part of the permittivity (right) of the different poly(2-oxazoline)s.

The value of the real part of the permittivity of all poly(2-oxazoline) is similar to the one of epoxy resins, with a value of approx. 4.63. Upon the addition of commercial SiO₂ and SiO₂-MPTMS nanoparticles, the real part of the permittivity is decreased to 4-4.2.

Table 11: Real and imaginary part of the permittivity of the poly(2-oxazoline)s at 40 Hz and 20 °C.

Polymer / Nanocomposite	ϵ'	ϵ''
Polyoxazoline 1	4.63	0.441
Polyoxazoline 2	3.96	0.261
Polyoxazoline 3	4.20	0.395

As observed for the other polymer systems the dielectric loss increases with decreasing frequencies (Figure 43). The dielectric loss of the dry poly(2-oxazoline)s is similar for Polyoxazoline 1 and Polyoxazoline 3 – fitting with the trend already observed for the epoxy resins and the polysiloxanes. For the wet poly(2-oxazoline)s, the dielectric loss is the lowest for Polyoxazoline 3, which also corresponds quite well with the trends observed for the epoxy resins and the polysiloxanes. The dielectric losses of the poly(2-oxazoline)s are summarized in Table 12.

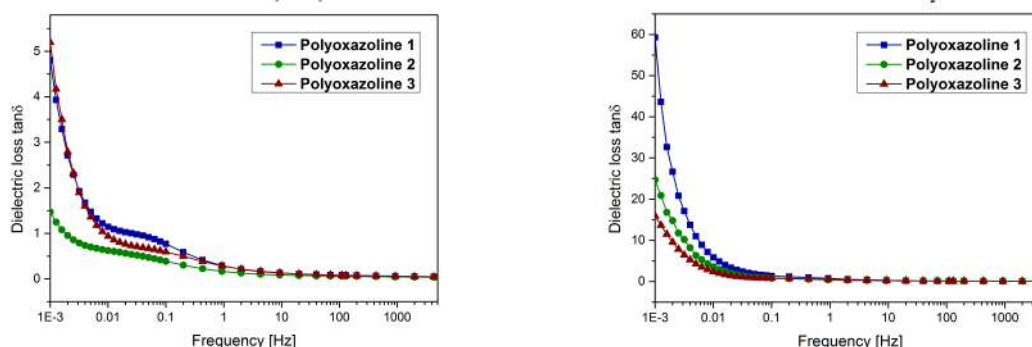


Figure 43: Dielectric loss of the dry (left) and wet (right) poly(2-oxazoline)s.

Table 12: Dielectric loss of the different poly(2-oxazoline)s at 40 Hz and 20 °C

Polymer / Nanocomposite	$\tan\delta_{\text{dry}}$	$\tan\delta_{\text{wet}}$	$\tan\delta_{\text{wet}} : \tan\delta_{\text{dry}}$
Polyoxazoline 1	0.0952	0.1640	1.72
Polyoxazoline 2	0.0659	0.1340	2.03
Polyoxazoline 3	0.0942	0.1463	1.55

As observed for the other polymer systems, the ratio dry:wet is the highest for Polyoxazolin 2 with 2.03 (Table 12). Interestingly, the ratio of Polyoxazoline 3 is lower than that of Polyoxazoline 1, which was not observable for the other two polymer systems. In summary, also for the poly(2-oxazoline)s, Polyoxazoline 3 shows a significant improvement concerning the dielectric loss of a wet nanocomposite.

In summary, for all three different polymer systems, a decrease in dielectric loss was achieved with the covalent embedment of the SiO₂-MPTMS nanoparticles compared to the nanocomposites filled with commercial SiO₂.

5. Conclusions

Nanodielectrics are materials that commonly consist of a polymer matrix mixed with nanofillers. With the addition of the nanoparticles into the polymer matrix, the dielectric properties of the material change. In order to investigate the influence of the nanoparticles on the properties of a polymer matrix, three different polymer systems were chosen for this study:

- an epoxy resin based on Bisphenol A diglycidyl ether DGEBA, cured with diethylenetriamine DETA,
- a poly(2-oxazoline)-based copolymer pNonOx₈₀-*stat*-pDec⁺Ox₂₀, composed of 2-nonyl-2-oxazoline NonOx and 2-decenyl-2-oxazoline Dec⁺Ox,
- a polysiloxane based on 1,3-divinyltetramethyldisiloxane Di⁺Siloxane, cured with a mixture of 2,2'-(ethylenedioxy)diethanethiol and trimethylolpropane-tris(3-mercaptopropionate).

Aside from the polymers, silica particles with a size of 5-15 nm were chosen as nanofillers, due to the high presence of hydroxy groups on their surface (Figure 44).

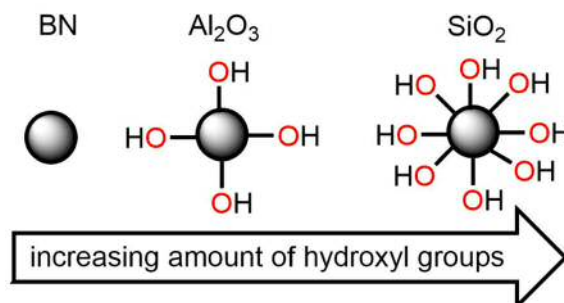


Figure 44: Amount of hydroxy groups present on a nanoparticles surface.

Since not only the influence of blended-in nanoparticles, but also the effect of their covalent attachment into the polymer matrix should be investigated, the functionalization of the silica's surface was performed with a silane coupling agent. The functionalized SiO₂-MPTMS nanoparticles were characterized with infrared spectroscopy, thermogravimetric analysis, pyrolysis and zeta-potential measurements. With these characterization methods, the successful functionalization of the SiO₂ nanoparticle was demonstrated.

Benefiting from this thiol functionality, UV-induced thiol-ene click-reactions were performed for the covalent embedment of the nanoparticles into the three different polymer matrices. The covalent bonds present between the polymer matrices and the nanoparticles are shown in Figure 45; in summary, this yields nine different samples (Table 13).

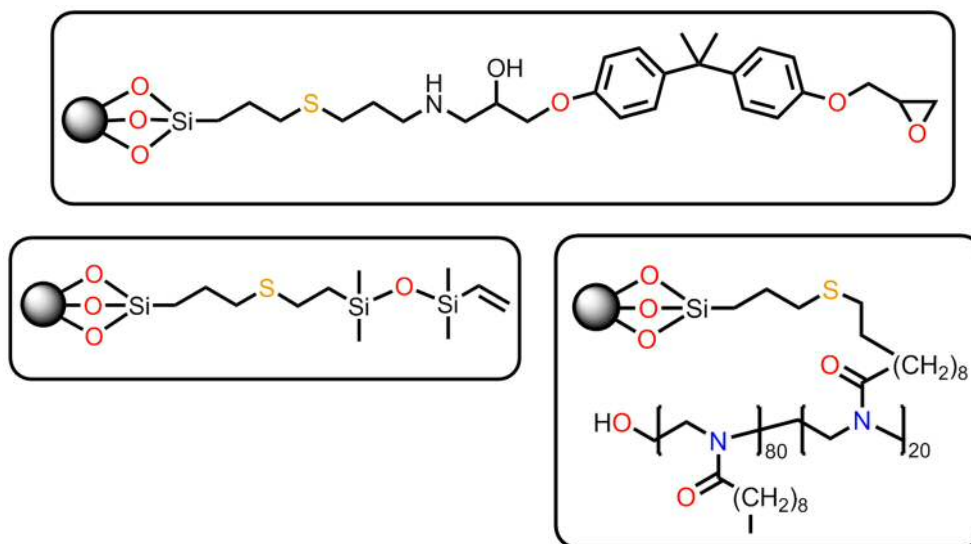


Figure 45: Covalent Embedment of the SiO₂-MPTMS nanoparticles in the different polymer matrices.

Table 13: Different kind of polymers and composites used for this investigation.

Polymer	Unfilled	5 wt.-% SiO ₂	5 wt.-% SiO ₂ -MPTMS
DGEBA	Epoxy Resin 1	Epoxy Resin 2	Epoxy Resin 3
pNonOx ₈₀ -stat-pDec ^o Ox ₂₀	Polyoxazoline 1	Polyoxazoline 2	Polyoxazoline 3
Di ^o Siloxane	Polysiloxane 1	Polysiloxane 2	Polysiloxane 3

Differential scanning calorimetry was performed to investigate the difference concerning the curing kinetics and curing processes in the unfilled polymers and the different nanocomposites. Whereas for the epoxy resins, no changes concerning the heat flow curves could be determined, the measurements revealed additional peaks in case of the polysiloxanes and the poly(2-oxazoline)s (Figure 46). The calculation of the activation energies according to Kissinger revealed lower values for the nanocomposites containing commercial SiO₂ nanoparticles due to catalytic activity of the present hydroxy groups. Furthermore, the lowering of the activation energy in case of Epoxy Resin 3 leads to the assumption that the covalent embedment of the SiO₂-MPTMS nanoparticles is present in the same temperature range as the curing reaction.

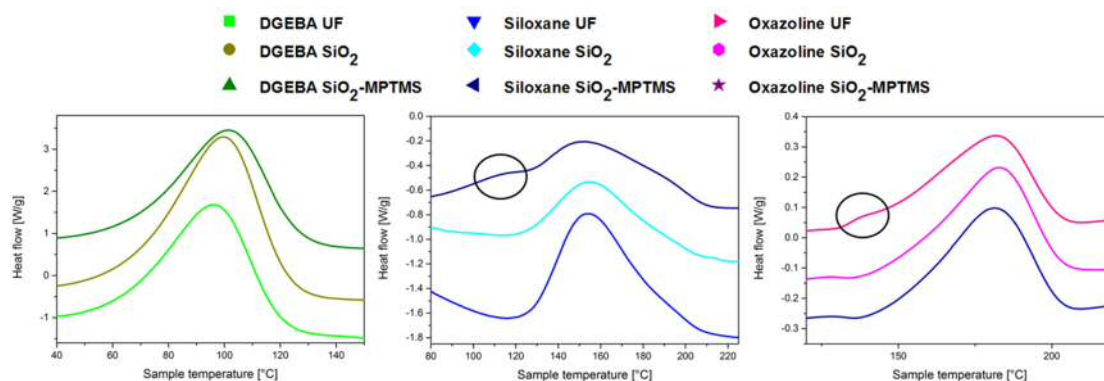


Figure 46: Heat flow vs. sample temperature curves for all unfilled polymers and nanocomposites.

Aside from the curing kinetics, also the agglomeration of the nanoparticles in the different polymer matrices was investigated by transmission electron microscopy. The covalent embedment of the nanoparticles led to decreased agglomeration of the SiO₂-MPTMS nanoparticles in the polymer matrices. This effect was clearly observed in case of Epoxy Resin 3 (Figure 47), Polyoxazoline 3, and Polysiloxane 3.

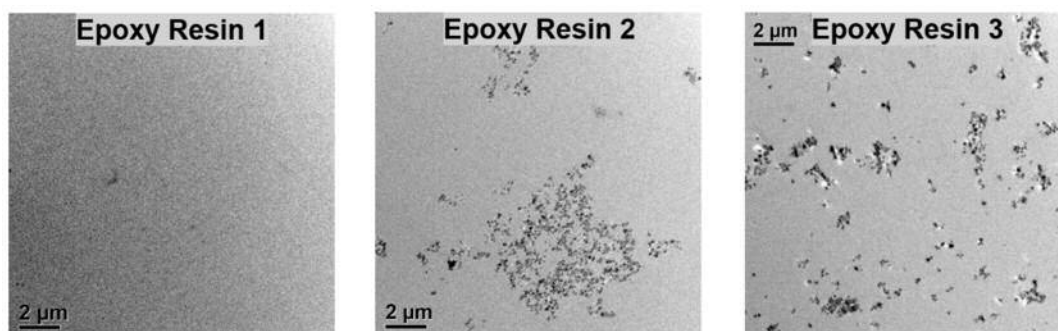


Figure 47: TEM pictures of the Epoxy Resins 1-3 at a magnification of 6500.

Additionally, the thermal conductivity of each sample was determined. No significant influence on the thermal conductivity could be identified for all three polymer systems.

For further characterization, the time-dependent water uptake of the various samples was determined. The nine samples were stored in a climate chamber at 30 °C and 85% humidity for 30 d (Figure 48). The water uptake decreased due to the addition of the commercial SiO₂ nanoparticles for every polymer system. In case of SiO₂-MPTMS, the polymer systems behaved differently. For Polyoxazoline 3, the water uptake was similar to that of Polyoxazoline 2, while it was comparably higher for

Epoxy Resin 3 and Polysiloxane 3. In fact, the water uptake of these two nanocomposites was more similar to the one of the unfilled polymers than to the nanocomposites filled with commercial SiO₂. This difference between the poly(2-oxazoline)s and the other two polymers could be explained by the distribution of the SiO₂-MPTMS nanoparticles in the nanocomposites as observed in the TEM images.

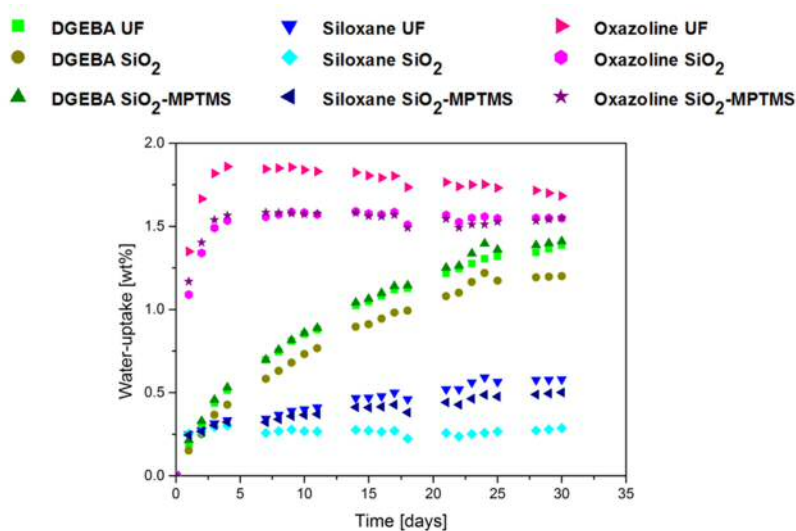


Figure 48: Time-dependent water uptake of the unfilled polymers and the different nanocomposites at a temperature of 30 °C and a humidity of 85%.

Since the water uptake can have a great impact on the performance of nanodielectrics, the permittivity and dielectric loss of all test specimens were determined in dry and wet state. The dielectric loss of the unfilled polymers and the different nanocomposites was determined at a temperature of 20 °C and a frequency of 50 Hz (industrial standard; Table 14).

For each polymer system, the same trend is observable: With the addition of commercial SiO₂ nanoparticles, the dielectric loss increases the most, leading to a decrease of the insulating properties for all of these nanocomposites. In comparison, with the covalent embedment of the nanoparticles, the dielectric loss was significantly lower. In conclusion, it may be argued that the covalent embedment leads to an increase of the insulating properties of wet nanocomposites in comparison to the ones filled with commercial SiO₂. In summary, for a better performance of nanodielectrics, the covalent embedment of nanoparticles seems to be a good choice concerning the dielectric properties.

Table 14: Dielectric loss of the unfilled polymers and different nanocomposites in dry and wet state (20 °C, 50 Hz).

	$\tan\delta_{\text{dry}}$	$\tan\delta_{\text{wet}}$	$\tan\delta_{\text{wet}}: \tan\delta_{\text{dry}}$
Epoxy Resin 1	0.0065	0.0091	1.40
Epoxy Resin 2	0.0115	0.0629	5.47
Epoxy Resin 3	0.0068	0.0198	2.91
Polysiloxane 1	0.0381	0.1114	2.92
Polysiloxane 2	0.0142	0.1953	13.76
Polysiloxane 3	0.0663	0.1937	2.92
Polyoxazoline 1	0.0952	0.1640	1.72
Polyoxazoline 2	0.0659	0.1340	2.03
Polyoxazoline 3	0.0942	0.1463	1.55

6. Abstract

The aim of this master thesis was to observe the dielectric properties of different polymer matrices filled with silica nanoparticles. Detailed investigations addressed the difference in the dielectric properties if the silica nanoparticles were covalently embedded into the polymer matrices or just blended into it. Three different polymer systems were chosen. The first one was based on Bisphenol A diglycidyl ether that was cured with diethylenetriamine. The second one was based on poly(2-nonyl-2-oxazoline)-*stat*-poly(2-dec-9'-enyl-2-oxazoline), which was cured via the thiol-ene click-reaction with a trithiol. The third one was based on 1,3-divinyltetramethyldisiloxane, which was cured by the thiol-ene click reaction with a mixture of dithiols and trithiols.

For the covalent embedment, the silica nanoparticles were functionalized with the silane coupling agent mercaptopropyl trimethoxysilane, adding a thiol functionality on the nanoparticles' surfaces. This thiol functionality could react with the double bonds in case of the poly(2-oxazoline) and the polysiloxane. For the covalent embedment in the epoxy resin, allylamine was used as a linker.

For the unfilled polymers, the nanocomposites blended with silica nanoparticles, and the nanocomposites with covalently embedded silica nanoparticles, numerous characterizations were performed. Whereas the covalent embedment did not show any change of the thermal conductivity of the test specimens, the water uptake and the dielectric loss were affected: The water uptake was lowered for the epoxy resin and the polysiloxane upon blending with non-functionalized silica particles, whereas the covalent embedment yielded a similar water uptake like for the unfilled polymers. In case of the poly(2-oxazoline)s, the water uptake for both types of filled nanocomposites was similar, whereas the one for the unfilled poly(2-oxazoline) was higher. Concerning the dielectric loss, for every polymer system the same trend was observable: With the covalent embedment of the nanoparticles, the dielectric loss of the wet nanocomposites could be decreased compared to the nanocomposites that were just blended with silica. Consequently, the covalent embedment leads to increased insulating properties in the case of humid/wet nanocomposites.

7. Kurzfassung

Das Ziel dieser Masterarbeit war es, die dielektrischen Eigenschaften verschiedener mit Silika-Nanopartikeln gefüllter Polymeren zu untersuchen. Insbesondere wurden die dielektrischen Eigenschaften in Abhängigkeit von der kovalenten Anbindung der Silika-Nanopartikel in die Polymermatrizen betrachtet. Zu diesem Zweck wurden drei verschiedene Polymersysteme ausgewählt. Das erste System war auf Basis des Bisphenol A-Diglycidylethers, der mit Diethylentriamin gehärtet wurde. Das zweite System war auf Basis des Poly(2-nonyl-2-oxazolin)-*stat*-poly(2-dec-9'-enyl-2-oxazolin), und das dritte basierte auf 1,3-Divinyltetramethyldisiloxan. Die beiden letzteren Systeme wurden beide über die Thiol-En Klick-Reaktion vernetzt.

Für die kovalente Einbettung wurden die Silika-Nanopartikel mit dem Silankopplungsreagenz Mercaptopropyltrimethoxysilan funktionalisiert, wodurch Thiolgruppen auf den Oberflächen der Nanopartikel angebracht werden. Diese Thiolgruppen können direkt mit den Doppelbindungen des Poly(2-oxazolin)s bzw. des Polysiloxans reagieren. Für die kovalente Einbettung in das Epoxidharz wurde Allylamin als Vernetzer verwendet.

Für die ungefüllten Polymere, die mit Silika-Nanopartikeln gefüllten Komposite und die Komposite mit kovalent eingebetteten Silika-Nanopartikeln wurden zahlreiche Charakterisierungen durchgeführt. Während sich durch die kovalente Einbettung keine Änderungen hinsichtlich der Wärmeleitfähigkeit der Komposite zeigten, wurden die Wasseraufnahme und der dielektrische Verlustfaktor verändert: Im Fall des Epoxidharzes und der Polysiloxane sank die Wasseraufnahme durch das Blenden mit Silika-Nanopartikeln, während sie sehr ähnlich für ungefüllte Polymere und die Komposite mit kovalent eingebetteten Silika-Nanopartikeln war. Bei den Poly(2-oxazolin)en war die Wasseraufnahme für beide Nanokomposite ähnlich, während die für das ungefüllte Poly-2-oxazolin höher war. Für den dielektrischen Verlustfaktor kann für jedes Polymersystem der gleiche Trend beobachtet werden: Mit der kovalenten Einbettung der Nanopartikel konnte der Verlustfaktor der nassen Nanokomposite im Vergleich zu den Kompositen mit beigemengten Silika-Nanopartikeln verringert werden. Folglich führte die kovalente Einbettung zur Erhöhung der Isoliereigenschaften für die nassen/feuchten Nanokomposite.

8. Materials and Methods

8.1. Used Chemicals

All chemicals were used as received, with the exception of methyl tosylate that distilled prior to use.

Substance	Deliverer	purity
10-undecenoic acid	Sigma-Aldrich, Austria	97%
1,3-divinyltetramethyldisiloxane	ABCR, Germany	98%
2,2'-(eEthylenedioxy)diethanethiol	Sigma-Aldrich, Austria	95%
acetonitrile	Carl Roth, Austria	99.5%
allylamine	Alfa Aesar	98%
Bisphenol A diglycidyl ether	ABCR, Germany	tech.
chloroform	VWR chemicals	99.4%
decanoic acid	SAFC	98%
diethylene triamine	Sigma-Aldrich, Austria	99%
ethanolamine	Sigma-Aldrich, Austria	98%
Lucirin TPO-L	ABCR, Germany	95%
mercaptopropyl-trimethoxy-silane	ABCR, Germany	95%
methoxy-2-propanol	Carl Roth, Austria	99%
methyl tosylate	Sigma-Aldrich, Austria	99%; distilled
<i>n</i> -Butylamine	Fluka Analytical	99.5%
Pentaerythritol-tetra(3-mercaptopropionate)	TCI	90%
SiO ₂ (particle size: 5 - 15 nm)	Sigma-Aldrich, Austria	99.5%
titanium(IV) butoxide	Sigma-Aldrich, Austria	99%
toluene	Sigma-Aldrich, Austria	98%
trimethylolpropane-tris(3-mercaptopropionate)	Sigma-Aldrich, Austria	95%

8.2. Analytical Methods

NMR measurements: All NMR measurements were performed with a Bruker Advance III 300 MHz spectrometer. Deuterated chloroform CDCl_3 was used as solvent. The residual signals were used as reference signals in case of ^1H -NMR and ^{13}C -NMR spectra (7.26 and 77 ppm, respectively).

Microwave-assisted synthesis: The microwave-assisted polymerization was performed with a Biotage Initiator 8 microwave reactor with auto sampler and internal infrared sensor.

Gel Permeation Chromatography: For the determination of the average molar mass of the polymers, GPC analyses were performed with a Merck Hitachi L-6000A pump, a column from Polymer Standards Service column (8\300 mm STV linear XL 5 μm grade size), and a differential refractometer Waters 410 detector. As solvent, a mixture of CHCl_3 : Et_3N : ^{15}O PrOH = 94:4 :2 was used.

IR measurements: Infrared spectroscopy was performed with an Alpha Fourier-Transform Infrared Spectrometer with ATR support. The background was determined before every measurement. The scan area was from 400-4000 cm^{-1} , and 48 scans were performed for each measurement.

Pyrolysis: The pyrolysis of the nanoparticles was performed with a Frontier Laboratories – Multi Shot Pyrolyser (PY-2020iD) coupled to a GC-MS QM2010 Plus from Shimadzu via an Optima-5-Accent column. The nanoparticles were pyrolyzed at 500 °C for 2 min and then transferred into the GC-MS system. The GC program was performed as follows: 50-90 °C with a heating rate of 10 $\text{K}\cdot\text{min}^{-1}$, hold 2 min at 90 °C, 90-300 °C with a heating rate of 10 $\text{K}\cdot\text{min}^{-1}$, hold for 2 min at 300 °C. Pyrolyzed species were ionized with an ionization energy of 70 eV.

Zeta-potential measurements: The zeta-potential measurements of the commercial SiO_2 nanoparticles and the SiO_2 -MPTMS nanoparticles were performed with an EKA ElectroKinetic Analyzer and the SurPASS Electrokinetic Analyzer from Anton Paar.

UV-induced crosslinking: The UV-induced crosslinking reactions were performed with an EFOS Novacure UV Hg/Xe Lamp of EXFO. The height and distance of the lamp to the test specimen was adjusted fitting for the different test specimen geometries. The energy of the UV-irradiation was 6 $\text{W}\cdot\text{cm}^{-2}$.

Panel press: For test specimen preparation of Polyoxazoline 1-3, a Collin P 200 PV panel press was used. A temperature of 190 °C and a pressure of 35 bar were applied.

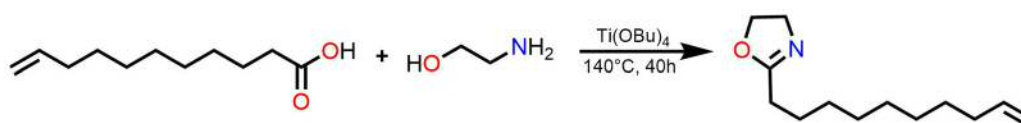
Differential Scanning Analysis: The curing process analysis was performed on a Mettler Toledo DSC 822e. For every polymer system, three different heating rates were used: 5, 10, and 20 K·min⁻¹. In all cases, double determination was performed. The heating range for the different systems was 25-200 °C in case of the epoxy resins, 60-230 °C in case of the polysiloxanes, and 50-250 °C in case of the poly(2-oxazoline)s. The determination of the glass-transition points was performed with a DSC 8500 from Perkin Elmer with a heating rate of 20 K·min⁻¹.

Thermal conductivity measurements: For the determination of the thermal conductivity, a DTC-300 conductivity meter was used.

Water uptake: For the time-dependent water uptake, the test specimens were stored in a Memmert HCP 108 chamber at a temperature of 30 °C and 85% humidity. The duration of the test was 30 d.

Dielectric characterization: Dielectric characterization was performed with a Spectano 100 from Omicron Lab. All samples were characterized in a frequency range of 1 mHz to 5 kHz.

8.3. Synthesis of 2-Dec-9'-enyl-2-oxazoline



Scheme 17: Synthesis of 2-dec-9'-enyl-oxazoline according to the Henkel-Patent.

150 mL of undecenoic acid (0.74 mol, 1.0 equiv.), 70 mL of ethanolamine (1.16 mol, 1.6 equiv.) and 1.3 mL of Ti(BuO)₄ (3.82 mmol, 0.005 equiv.) were placed in a 500 mL round bottom flask. The mixture was stirred under reflux overnight. After 20 and 24 h, 1.3 mL of Ti(BuO)₄ were added each time. The mixture was again stirred overnight. The reflux condenser was removed, and the mixture was stirred for another 12 h for water removal. The crude product was obtained via vacuum

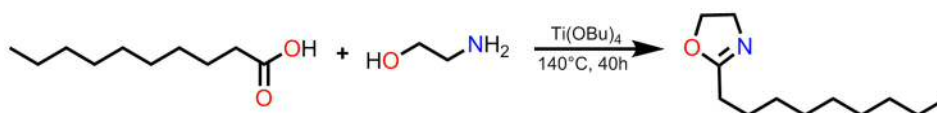
distillation (180 °C, 4 mbar), yielding a yellow liquid. For purification, column chromatography with chloroform was performed, yielding a colorless viscous liquid of Dec⁻Ox with a yield of 68.1% (105.50 g).

¹H NMR (300 MHz, CDCl₃): δ (ppm) = 1.23 (10 H, s), 1.53 (2 H, t), 1.93 (2 H, t), 2.16 (2 H, t), 3.71 (2 H, t), 4.11 (2 H, t), 4.84 (2 H, t), 5.72 (1 H, m).

¹³C NMR (75 MHz, CDCl₃): δ (ppm) = 22.9, 28.0, 29.2, 33.8, 54.4, 67.1, 114.1, 139.2, 168.6.

IR (ATR): ν (cm⁻¹) = 2924, 2853, 1668, 1640, 1461, 1432, 1385, 1361, 1227, 1167, 987, 952, 907, 723.

8.4. Synthesis of 2-Nonyl-2-oxazoline



Scheme 18: Synthesis of 2-nonyl-oxazoline according to the Henkel-Patent.

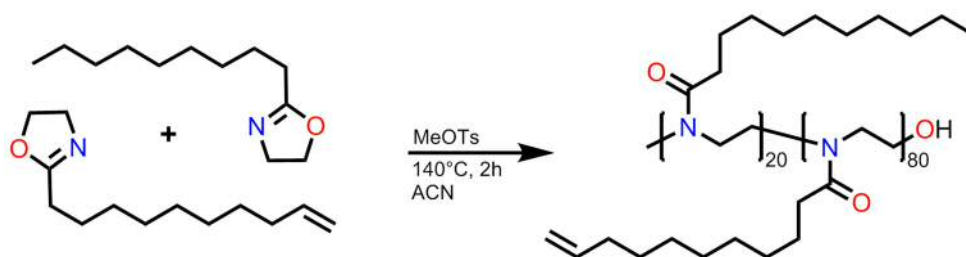
150 mL of decanoic acid (0.77 mol, 1.0 equiv.), 70 mL of ethanolamine (1.16 mol, 1.5 equiv.), and 1.3 mL of Ti(BuO)₄ (3.82 mmol, 0.005 equiv.) were placed in a 500 mL round bottom flask. The mixture was stirred under reflux overnight. After 20 and 24 h, 1.3 mL of Ti(BuO)₄ were added each time. The mixture was again stirred overnight. The reflux condenser was removed, and the mixture was stirred for another 12 h for water removal. The crude product was obtained via vacuum distillation (180 °C, 4 mbar), yielding a yellow liquid. Column chromatography with chloroform yielded a colorless viscous liquid of NonOx with a yield of 53.3% (80.92 g).

¹H NMR (300 MHz, CDCl₃): δ (ppm) = 0.78 (3H, t), 1.19 (12H, s), 1.53 (2H, t), 2.17 (2H, t), 3.72 (2H, t), 4.11 (2H, t).

¹³C NMR (75 MHz, CDCl₃): δ (ppm) = 14.1, 22.7, 26.0, 28.0, 29.3, 31.9, 54.4, 67.1, 168.7.

IR (ATR): ν (cm⁻¹) = 2923, 2854, 1688, 1464, 1362, 1231, 1165, 986, 950, 908, 754, 722.

8.5. Synthesis of Poly(2-nonyl-2-oxazoline)-*stat*-poly(2-dec-9'-enyl-2-oxazoline)



Scheme 19: Microwave-assisted statistical copolymerization of Dex⁻Ox and NonOx.

For the microwave assisted copolymerization, 0.5661 g of Dec⁻Ox (2.73 mmol, 2.0 equiv.), 2.1391 g of NonOx (10.95 mmol, 8.0 equiv.), 25.1 mg of methyl tosylate (0.13 mmol, 0.07 equiv.), and 2.5 mL of acetonitrile were placed in a microwave vial. The reaction in the microwave reactor was performed using the following conditions: 140 °C, 2 h, and medium absorption. After cooling, a white solid precipitated, which was dried at the rotary evaporator yielding a white powder of pNonOx₈₀-*stat*-pDec⁻Ox₂₀ with a yield of ≥ 99 % (2.72 g).

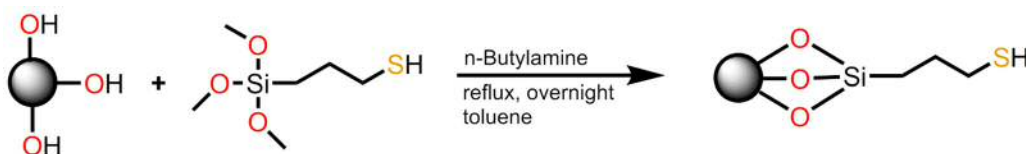
¹H NMR (300 MHz, CDCl₃): δ (ppm) = 0.79 (277 H), 1.20 (1340 H), 1.52 (244 H), 1.95 (52 H), 2.18 (230 H), 3.37 (400 H), 4.83 (46 H), 5.69 (23 H).

¹³C NMR (75 MHz, CDCl₃): δ (ppm) = 14.1, 22.6, 25.4, 28.9, 29.1, 29.3, 29.5, 31.9, 33.7, 43.2, 45.3, 114.1, 125.7, 128.8, 139.0, 173.1, 173.9.

IR (ATR): ν (cm⁻¹) = 2956, 2920, 2851, 1640, 1462, 1430, 1182, 1161, 909, 772, 721.

GPC: M_w = 13.5 kDa, M_n = 10.3 kDa; dispersity index = 1.31.

8.6. Functionalization of the Nanoparticles



Scheme 20: Surface functionalization of commercially available SiO₂ nanoparticles.

2.5 g of SiO₂ (particle size: 5-15 nm) were dispersed in 100 mL of toluene. 20 mL of mercaptopropyl trimethoxysilane and 0.05 mL of *n*-butylamine were added. The dispersion was stirred under reflux for 5 h. The functionalized nanoparticles SiO₂-MPTMS were obtained via centrifugation and washed with 50 mL of toluene three times. The nanoparticles were dried for 48 h at 110 °C.

IR (ATR): ν (cm⁻¹) = 1624, 1061, 959, 806, 700, 451.

8.7. Preparation of the Test Specimens

Three different polymer systems were used:

- an epoxy resin of Bisphenol A diglycidyl ether DGEBA, cured with diethylene triamine DETA
- a polysiloxane composed of 1,3-divinyltetramethyldisiloxane Di⁻Siloxane, cured with a mixture of 2,2'-(ethylenedioxy)diethanethiol and trimethylolpropane-tris(3-mercaptopropionate), and
- the poly(2-oxazoline) pNonOx₈₀-*stat*-pDec⁻Ox₂₀, cured with pentaerythritol-tetra(3-mercaptopropionate).

In every case test specimens of:

- the unfilled polymer,
- the polymer filled with 5 wt.-% of commercial SiO₂ nanoparticles, and
- the polymer filled with 5 wt.-% of SiO₂-MPTMS nanoparticles

were prepared.

Two different kinds of test specimens were prepared:

- circular test specimens with 2 mm height & 50 mm diameter, and
- square foils with lengths of 80 mm & heights between 100-400 μm.

8.7.1. Epoxy Resin-based Specimens

For the manufacturing of the test specimens, 5 equiv. of DGEBA were mixed with 2 equiv. of DETA in a 20 mL vial. In case of the nanocomposites, the commercial SiO₂ and SiO₂-MPTMS nanoparticles were dispersed in the epoxy resin by sonication for

10 min and additional stirring by prior to the addition of the curing agent DETA. For covalent embedment of the SiO₂-MPTMS nanoparticles, also allylamine and the photoinitiator TPO-L were added. Circular test specimens were prepared by transferring the mixture in a steel template and subsequent curing at 90 °C for 3 hours. Square foils were prepared by transferring the mixture on a PP-foil and subsequent curing at 90 °C for 30 minutes.

8.7.2. Polysiloxane-based Specimens

For the manufacturing of the test specimens, 15 equiv. of Di⁻Siloxane were mixed with 9 equiv. of 2,2'-(ethylenedioxy)diethanethiol and 4 equiv. of trimethylolpropane-tris(3-mercaptopropionate). In case of the nanocomposites, the commercial SiO₂ and SiO₂-MPTMS nanoparticles were dispersed in the mixture by sonication for about 20 min. 5 wt.-% of the photoinitiator TPO-L were added, and the mixture was again sonicated for 60 s. Circular test specimens were prepared by transferring the mixture in a steel template and subsequent irradiation with UV-light (254 nm, 6 W·cm⁻²) for 20 min. Square foils were prepared by transferring the mixture on a PP foil and subsequent irradiation with UV-light (254 nm, 6 W·cm⁻²) for 60 s. In both cases, post-baking was performed in a drying oven at 90 °C for 2 hours.

8.7.3. Poly(2-oxazoline)-based Specimens

For the manufacturing of the circular test specimens, pNonOx₈₀-*stat*-pDec⁻Ox₂₀ was fine crushed in a mortar. In case of the nanocomposites, the commercial SiO₂ and SiO₂-MPTMS nanoparticles were added prior to the addition of the stoichiometric amount of pentaerythritol-tetra(3-mercaptopropionate) and 5 wt.-% of the photoinitiator TPO-L. The reaction mixture was transferred in a steel template and platen pressed at 190 °C and 35 bar for 1 h. For the manufacturing of the square test specimens, pNonOx₈₀-*stat*-pDec⁻Ox₂₀ was dissolved in a 1:1 mixture of toluene and methoxypropanol. The SiO₂ and SiO₂-MPTMS nanoparticles were sonicated in the solution before adding 1 equiv. of the curing agent pentaerythritol-tetra(3-mercaptopropionate) and 5 wt.-% of the photoinitiator TPO-L. The solution was transferred on a PP foil and irradiated with UV-light (254 nm, 6 W·cm⁻²) for 60 s.

9. References

- [1] M. Wietschel, M. Arens, C. Dötsch, S. Herkel, W. Krewitt, P. Markewitz, D. Möst, M. Scheufen: Energietechnologien 2050 – Schwerpunkte der Forschung und Entwicklung. *Technologiebericht Fraunhofer Verlag*, **2010**.
- [2] T. Tanaka: Dielectric Nanocomposites with Insulating Properties. *IEEE Trans. Dielectr. Electr. Insul.* **2005**, 5, 914.
- [3] R. Hackam: Outdoor HV Composite Polymeric Insulators. *IEEE Trans. Dielectr. Electr. Insul.* **1999**, 6, 557.
- [4] A. Jaya, H. Berahim, T. Tumiran, R. Rochimadi: Accelerated Aging Effect on Epoxy-polysiloxane-Rice Husk Ash Polymeric Insulator Material. *Electr. Electron. Eng.* **2012**, 2, 208.
- [5] M. F. Frechette, M. L. Trudeau, H. D. Alamdari, S. Boily: Introductory Remarks on Nanodielectrics. *IEEE Trans. Dielectr. Electr. Insul.* **2004**, 5, 808.
- [6] T. Hanemann, D. V. Szabo: Polymer-Nanoparticle Composites: From Synthesis to Modern Applications. *Materials* **2010**, 3, 3486.
- [7] R. Marenbach, D. Nelles, C. Tuttas: Elektrische Energietechnik. *Springer Fachmedien Wiesbaden*, **2013**.
- [8] B. S. Rubin: Bisphenol A: An Endocrine Disruptor with Widespread Exposure and Multiple Effects. *J. Steroid Biochem. Mol. Biol.* **2011**, 127, 27.
- [9] L. N. Vandenberg, R. Hauser, M. Marcus, N. Olea, W. V. Welshons: Human Exposure to Bisphenol A (BPA). *Reprod. Toxicol.* **2007**, 24, 139.
- [10] European Commission, Proposed Ban on the Use of Two-Component Epoxy Containing Bisphenol A or Bisphenol A Diglycidyl Ether in the Moulding of New Plastic Pipes Inside Existing Water Supply Pipes, **2016**.
- [11] E. Rossegger, V. Schenk, F. Wiesbrock: Design Strategies for Functionalized Poly(2-oxazoline)s and Derived Materials. *Polymers* **2013**, 5, 956.
- [12] M. Fimberger, I. A. Tsekmes, R. Kochetov, J. J. Smit, F. Wiesbrock: Crosslinked Poly(2-oxazoline)s as “Green” Materials for Electronic Applications. *Polymers*, **2016**, 8, 6
- [13] A. Eibel, P. Marx, H. Jin, I. A. Tsekmes, I. Mühlbacher, J. J. Smit, W. Kern, F. Wiesbrock, Enhancement of the Insulation Properties of Poly(2-oxazoline)-co-Polyester Networks by the Addition of Nanofillers. *Macromol. Rapid Commun.* **2018**, 39, 1700681 (5 p.).
- [14] P. Marx, A. Wanner, Z. Zhang, H. Jin, I. A. Tsekmes, J. Smit, W. Kern, F. Wiesbrock: Effect of Interfacial Polarization and Water Absorption on the Dielectric Properties of Epoxy-Nanocomposites. *Polymers* **2017**, 9, 195.

- [15] G. C. Psarras: Hopping conductivity in polymer matrix-metal particles composites. *Composites Part A* **2006**, 37, 1545.
- [16] Y. Cao, P. C. Irwin: Electrical Conduction in Polyimide Nanocomposites. *IEEE Conf. Electr. Insul. Dielectr. Phenomena* **2003**, 116.
- [17] T. J. Lewis: Nanometric Dielectrics. *IEEE Trans. Dielect. Electr. Insul.* **1994**, 5, 812.
- [18] E. I. Izorodina, M. Forsyth, D. R. Macfarlane: On the Components of the Dielectric Constants of Ionic Liquids: Ionic Polarization? *Phys. Chem. Chem. Phys.* **2009**, 11, 2452.
- [19] E. Kuffel, W. S. Zaengl, J. Kuffel: Non-Destructive Insulation Test Techniques. *High Volt. Eng. Fundam.* **2000**, 395.
- [20] C. T. Dervos, C. D. Paraskevas, P. D. Skafidas, P. Vassiliou: A Complex Permittivity Based Sensor for the Electrical Characterization on High-Voltage Transformer Oils. *Sensors* **2005**, 5, 302.
- [21] F. Hussain, J. Chen, M. Hojjati: Epoxy-Silicate Nanocomposites: Cure Monitoring and Characterization. *Mater. Sci. Eng. A.* **2007**, 5, 445.
- [22] J. K. Nelson, J. C. Fothergrill, L. A. Dissado, W. Peasgood: Towards an Understanding of Nanometric Dielectrics. *IEEE Conf. Electr. Insul. Dielectr. Phenomena* **2002**, 295.
- [23] J. K. Nelson, Y. Hu, J. Thiticharoenpong: Electrical Properties of TiO₂ Nanocomposites. *IEEE Conf. Electr. Insul. Dielectr. Phenomena* **2003**, 719.
- [24] J. K. Nelson, Y. Hu: Nanocomposite Dielectrics – Properties and Implications. *Appl. Phys.* **2005**, 38, 213.
- [25] J. K. Nelson, J. C. Fothergill: Internal Charge Behavior of Nanocomposites. *Nanotechnology* **2004**, 15, 586.
- [26] T. Tanaka, M. Kozako, N. Fuse, Y. Ohki: Proposal of a Multi-Core Model for Polymer Nanocomposite Dielectrics. *IEEE Trans. Dielectr. Electr. Insul.* **2005**, 12, 669.
- [27] H. Gu, C. Ma, J. Gu, J. Guo, X. Yan, J. Huang, Q. Zhang, Z. Guo: An Overview of Multifunctional Epoxy Nanocomposites. *J. Mater. Chem. C* **2016**, 4, 5890.
- [28] M. Roy, J. K. Nelson, R. K. MacCrone, L. S. Schadler: Polymer Nanocomposite Dielectrics – The Role of the Interface. *IEEE Trans. Dielectr. Electr. Insul.* **2005**, 12, 629.
- [29] R. C. Anderson, R. S. Muller, C. W. Tobias: Chemical Surface Modification of Porous Silicon. *J. Electrochem. Soc.* **1993**, 140, 1393.
- [30] E. P. Plueddemann, H. A. Clark, L. E. Nelson, K. R. Hoffmann: Silane Coupling Agents for Reinforced Plastics. *Mod. Plast.* **1962**, 39, 135.
- [31] J. Zhao, M. Milanova, M. M. C. G. Warmoeskerken, V. Dutschk: Surface Modification of TiO₂ Nanoparticles with Silane Coupling Agents. *Colloids Surf.* **2012**, 413, 273.

- [32] F. Ahangaran, A. Hassanzadeh, S. Nouri: Surface Modification of Fe₃O₄@SiO₂ Microsphere by Silane Coupling Agent. *Int. Nano Lett.* **2013**, 3, 1.
- [33] L. A. S. A. Prado, M. Sriyai, M. Ghislandi, A. Barros-Timmons, K. Schulte: Surface Modification of Alumina Nanoparticles with Silane Coupling Agents. *J. Braz. Chem. Soc.* **2010**, 21, 2238.
- [34] M. Iijima, S. Takenouchi, I. W. Lenggoro, H. Kamiya: Effect of Additive Ratio of Mixed Silane Alkoxides on Reactivity with TiO₂ Nanoparticle Surface and their Stability in Organic Solvents. *Adv. Powder Technol.* **2011**, 22, 663.
- [35] T. W. Dalkin: Application of Epoxy Resins in Electrical Apparatus. *IEEE Trans. Electr. Insul.* **1974**, 4, 121.
- [36] J. Alexander, T. Bertolini: Epoxide Reactions. *J. Chem. Educ.* **2002**, 79, 1.
- [37] R. B. Munn: Electric Power Generator and System. US-Patent 4.475.075, **1984**.
- [38] W. Browstow, W. Chonkaew, K. P. Menard, T. W. Scharf: Modification of an Epoxy Resin with a Fluoroepoxy Oligomer for Improved Mechanical and Tribological Properties. *Mater. Sci. Eng. A.* **2009**, 507, 241.
- [39] B. Denq, Y. Hu, L. Chen, W. Chiu, T. Wu: The Curing Reaction and Physical Properties of DGEBA/DETA Epoxy Resin Blended with Propyl Ester Phosphazane. *J. Appl. Polym. Sci.* **1999**, 74, 229.
- [40] M. G. Danias, K. Varsamidou, Y. Cheng, A. D. Karlis: Epoxy Resin Insulation: The Influence of Nanoparticles of the Flashover Voltage and Possible Alternatives for Electrical Machines Insulation. *XXII Int. Conf. Electr. Machines* **2016**, 1668.
- [41] H. Couderc, M. Frechette, S. Savoie, M. Reading, A. S. Vaughan: Dielectric and Thermal Properties of Boron Nitride and Silica Epoxy Composites. *IEEE Int. Symp. Electr. Insul.* **2012**, 64.
- [42] J. Gu, X. Yang, Z. Lv, N. Li, C. Liang, Q. Zhang: Functionalized Graphite Nanoplatelets/Epoxy Resin Nanocomposites with High Thermal Conductivity. *Int. J. Heat Mass Transfer* **2016**, 92, 15.
- [43] G. Iyer, R. S. Gorur, R. Richert, A. Krivda, L. E. Schmidt: Dielectric properties of epoxy based nanocomposites for high voltage insulation. *IEEE Trans. Dielectr. Electr. Insul.* **2011**, 18, 659.
- [44] M. G. Danikas, T. Tanaka: Nanocomposites – a Review of Electrical Treeing and Breakdown. *IEEE Electr. Insul. Mag.* **2009**, 25, 19.
- [45] S. Singha, M. J. Thomas: Dielectric Properties of Epoxy Nanocomposites. *IEEE Trans Dielectr. Electr. Insul.* **2008**, 15, 12.
- [46] H. Schlaad, R. Hoogenboom: Poly(2-oxazoline)s and Related Pseudo-Polypeptides. *Macromol. Rapid Commun.* **2012**, 33, 1599.
- [47] B. Verbraeken, B. D. Monnery, K. Lava, R. Hoogenboom: The Chemistry of Poly(2-oxazoline)s. *Eur. Polym. J.* **2017**, 88, 451.

- [48] S. Gabriel: Zur Kenntnis der Bromäthylamins. *Ber. Dtsch. Chem. Ges.* **1889**, 22, 1139.
- [49] A. Gress, A. Völkel, H. Schlaad: Thiol-Click Modification of Poly[2-(3-butenyl)-2-oxazoline]. *Macromolecules* **2007**, 40, 7928.
- [50] T. R. Dargville, K. Lava, B. Verbraeken, R. Hoogenboom: Unexpected Switching of the Photogelation Chemistry in Crosslinked Poly(2-oxazoline) Copolymers. *Macromolecules* **2016**, 49, 4774.
- [51] H. Witte, W. Seeliger: Cyclische Imidsäureester aus Nitrilen und Aminoalkoholen. *Justus Liebigs Ann. Chem.* **1974**, 996.
- [52] H. J. Krause, P. Neumann: Verfahren zur Herstellung von 2-Alkyl- bzw. 2-Alkenyloxazolinen. *EP0315856*, **1995**.
- [53] C. Petit, K. P. Luef, M. Edler, T. Griesser, J. M. Kremsner, A. Stadler, B. Grassl, S. Reynaud, F. Wiesbrock: Microwave-Assisted Syntheses in Recyclable Ionic Liquids: Photoresist Based on Renewable Resources. *ChemSusChem*. **2015**, 8, 3401.
- [54] W. Seelinger, E. Ausderhaar, W. Diepers, R. Reinauer, R. Nehring, W. Thier, H. Hellmann: Recent Syntheses and Reactions of Cyclic Imidic Esters. *Angew. Chemie Int. Ed.* **1966**, 5, 875.
- [55] D. A. Tomalia, D. P. Sheetz: Homopolymerization of 2-Alkyl- and 2-Aryl-2-oxazolines. *J. Polym. Sci. Part A: Polym. Chem.* **1966**, 4, 2253.
- [56] T. Kagiya, T. Maeda, K. Fukui, S. Narisawa: Ring Opening Polymerization of 2-Substituted 2-Oxazolines. *Polym. Lett.* **1966**, 4, 441.
- [57] A. Levy, M. Litt: Polymerization of Cyclic Imino Ethers I. Oxazolines. *Polym. Lett.* **1967**, 5, 871.
- [58] F. Wiesbrock, R. Hoogenboom, C. H. Abeln, U. S. Schubert: Single-Mode Microwave Ovens as New Reaction Devices: Accelerating the Living Polymerization of 2-Ethyl-2-Oxazoline. *Macromol. Rapid Commun.* **2005**, 26, 160.
- [59] F. Wiesbrock, R. Hoogenboom, M. Leenen, S. F. G. M. Van Nipsen, M. Van der Loop, C. H. Abeln, A. M. J. Van Der Berg, U. S. Schubert: Microwave-Assisted Synthesis of a 4²-Membered Library of Diblock Copoly (2-oxazoline)s and Chain-Extended Homo Poly(2-oxazoline)s and their Thermal Characterization. *Macromolecules* **2005**, 38, 7957.
- [60] C. Ebner, T. Bodner, F. Stelzer, F. Wiesbrock: One Decade of Microwave-Assisted Polymerizations: Quo Vadis? *Macromol. Rapid Commun.* **2011**, 32, 254.
- [61] M. Fimberger, K. Luef, C. Payert, R. Fischer, F. Stelzer, M. Kallay, F. Wiesbrock: The pi-Electron Delocalization in 2-Oxazolines Revisited: Quantification and Comparison with its Analogue in Esters. *Materials* **2015**, 8, 5383.
- [62] C. E. Hoyle, C. N. Bowman: Thiol-En-Klickchemie. *Angew. Chem.* **2010**, 122, 1584.

- [63] H. C. Kolb, M. G. Finn, K. B. Sharpless: Click Chemistry: Diverse Chemical Function from a few good Reactions. *Angew. Chemie Int. Ed.* **2001**, *40*, 2004.
- [64] M. Fimberger, V. Schenk, E. Rossegger, F. Wiesbrock: UV-Induced Crosslinking of Poly[2-(2'-Norborenyl)-2-oxazoline]s, *Period. Polytech. Chem. Eng.* **2014**, *58*, 69.
- [65] C. S. Subhas, P. Shah: A Review on Silicone Rubber, *Natl. Acad. Sci. Lett.* **2013**, *36*, 355.
- [66] D. Troegel, J. Stohrer: Recent Advances and Actual Challenges in Late Transition Metal Catalyzed Hydrosilylation of Olefins from an Industrial Point of View, *Coord. Chem. Rev.* **2011**, *255*, 1440.
- [67] E. G. Rochow: The Direct Synthesis of Organosilicon Compounds, *J. Am. Chem. Soc.* **1945**, *67*, 963.
- [68] B. D. Karstedt: Platinum Complexes of Unsaturated Siloxanes and Platinum Containing Organopolysiloxanes, *US3775452 A*, **1973**.
- [69] M. A. Schroeder, M. S. Wrighton: Pentacarbonyliron(0) Photocatalyzed Reactions of Trialkylsilanes with Alkenes, *J. Organomet. Chem.* **1977**, *128*, 345.
- [70] S. Sakaki, N. Mizoe, M. Sugimoto: Theoretical Study of Platinum(0)-Catalyzed Hydrosilylation of Ethylene. Chalk-Harrod Mechanism or Modified Chalk-Harrod Mechanism, *Organometallics*, **1998**, *17*, 2510.
- [71] L. Peng, W. Qisui, L. Xi, Z. Chaocan: Investigation of the States of Water and OH Groups on the Surface of Silica. *Colloids Surf. A: Physicochem. Eng. Asp.* **2009**, *334*, 112.
- [72] P. Nedeljko, M. Turel, A. Kosak, A. Lobnik: Synthesis of Hybrid Thiol-Functionalized SiO₂ Particles Used for Agmatine Determination. *J. Sol-Gel Sci. Technol.* **2016**, *79*, 487.
- [73] P. E. Sanchez-Jimenez, J. M. Criado, L. A. Perez-Maqueda: Kissinger: Kinetic Analysis of Data Obtained under Different Heating Schedules. *J. Therm. Anal. Calorim.* **2009**, *94*, 427.
- [74] S. Hoepfener, F. Wiesbrock, R. Hoogenboom, H. M. L.Thijs, U. S. Schubert: Morphologies of Spin-Coated Films of a Library of Diblock Copoly(2-oxazoline)s and Their Correlation to the Corresponding Surface Energies. *Macromol. Rapid Commun.* **2006**, *27*, 405.

10. Appendix

10.1. List of Abbreviations

Bisphenol A diglycidyl ether	DGEBA
chloroform (deuterated)	CDCl ₃
2-decenyl-2-oxazoline	Dec ^o Ox
diethylenetriamine	DETA
1,3-divinyltetramethyldisiloxane	Di ^o Siloxane
mercaptopropyltrimethoxysilane	MPTMS
2-nonyl-2-oxazoline	NonOx

10.2. List of Figures

Figure 1: Schematic representation of a nanocomposite.....	4
Figure 2: Multi-core model of nanoparticle-polymer interactions proposed by Tanaka et al. [26].....	7
Figure 3: Illustration of the different interactions between a nanoparticle and a polymer matrix: (a) Nearly no interaction. (b) Electrostatic or van-der-Waals interactions that lower the interspace. (c, d) Covalent bonds between the nanoparticle and the polymer matrix. [27]	8
Figure 4: Amount of hydroxy groups present on a nanoparticle's surface.	9
Figure 5: Functionalization of a nanoparticle's surface with a silane coupling agent. [31]	10
Figure 6: Structure of the epoxy functionality.....	10
Figure 7: Structure of DGEBA.	11
Figure 8: Monomer structure of 2-oxazolines with possible substituents. [11].....	13
Figure 9: ¹ H-NMR spectrum of Dec ^o Ox with signals assigned to the chemical structure.....	22
Figure 10: ¹ H-NMR spectrum of NonOx with signals assigned to the chemical structure.....	22
Figure 11: ¹ H-NMR spectrum of pNonOx ₈₀ -stat-pDec ^o Ox ₂₀ with signals assigned to the chemical structure.....	23

Figure 12: Infrared spectra of the commercially available SiO ₂ nanoparticles (black) and the SiO ₂ -MPTMS nanoparticles (blue).....	25
Figure 13: Thermogravimetric analysis of the commercial SiO ₂ nanoparticles (black) and the SiO ₂ -MPTMS nanoparticles (blue).....	25
Figure 14: Pyrolysis of the commercial SiO ₂ nanoparticles (black) and the SiO ₂ -MPTMS nanoparticles (blue).	26
Figure 15: Zeta-potential measurements of the commercial SiO ₂ nanoparticles (black) and SiO ₂ -MPTMS nanoparticles (blue).	27
Figure 16: Photography of test specimen of the different epoxy resins. Left: Epoxy Resin 1, middle: Epoxy Resin 2, right: Epoxy Resin 3. The diameter of the specimens is d = 50 mm.	28
Figure 17: Test specimen of the different polysiloxanes. Left: Polysiloxane 1, middle: Polysiloxane 2, right: Polysiloxane 3. The diameter of the specimens is d = 50 mm.	30
Figure 18: Test specimen of the different poly(2-oxazoline)s. Left: Polyoxazoline 1, middle: Polyoxazoline 2, right: Polyoxazoline 3. The diameter of the specimens is d = 50 mm.....	31
Figure 19: Heat flow vs. sample temperature curves and conversion curves of the different epoxy resins.....	33
Figure 20: Heat flow vs. sample temperature curves of the different polysiloxanes.	34
Figure 21: Conversion curves of the different polysiloxanes at different heating rates.	35
Figure 22: Heat flow vs. sample temperature curves of the different poly(2-oxazoline)s.	36
Figure 23: Conversion curves of the different poly(2-oxazoline)s at different heating rates.....	37
Figure 24: TEM pictures of Epoxy Resin 1-3 at a magnification of 6,500.	38
Figure 25: TEM pictures of Epoxy Resin 2-3 at a magnification of 30,000.	39
Figure 26: TEM picture of Epoxy Resin 3 at a magnification of 67,000.	39
Figure 27: TEM pictures of the Polysiloxanes 1-3 at a magnification of 6,500.....	40
Figure 28: TEM pictures of the Polysiloxanes 2-3 at a magnification of 30,000.....	40
Figure 29: TEM pictures of the Polyoxazolines 1-3 at a magnification of 6,500.....	41
Figure 30: TEM pictures of the Polyoxazolines 2-3 at a magnification of 30,000.....	41
Figure 31: TEM pictures of Polyoxazoline 1 at a magnification of 21,000.....	42

Figure 32: Thermal conductivity of Epoxy Resin 1-3 at temperatures of 30, 60, and 90 °C.	43
Figure 33: Thermal conductivity of Polysiloxane 1-3 at temperatures of 30, 60, and 90 °C.	43
Figure 34: Thermal conductivity of Polyoxazoline 1-3 at temperatures of 30, 60, and 90 °C.	44
Figure 35: Water uptake of Epoxy Resins 1-3 at a temperature of 30 °C and a humidity of 85%.	45
Figure 36: Water uptake of Polysiloxane 1-3 at a temperature of 30 °C and a humidity of 85%.	46
Figure 37: Water uptake of Polyoxazolines 1-3 at a temperature of 30 °C and a humidity of 85%.	47
Figure 38: Real part of the permittivity (left) and imaginary part of the permittivity (right) of the different epoxy resins.	48
Figure 39: Dielectric loss of the dry (left) and wet (right) epoxy resins.	50
Figure 40: Real part of the permittivity (left) and imaginary part of the permittivity (right) of the different polysiloxanes.	51
Figure 41: Dielectric loss of the dry (left) and wet (right) polysiloxanes.	52
Figure 42: Real part of the permittivity (left) and imaginary part of the permittivity (right) of the different poly(2-oxazoline)s.	53
Figure 43: Dielectric loss of the dry (left) and wet (right) poly(2-oxazoline)s.	54
Figure 44: Amount of hydroxy groups present on a nanoparticles surface.	55
Figure 45: Covalent Embedment of the SiO ₂ -MPTMS nanoparticles in the different polymer matrices.	56
Figure 46: Heat flow vs. sample temperature curves for all unfilled polymers and nanocomposites.	57
Figure 47: TEM pictures of the Epoxy Resins 1-3 at a magnification of 6500.	57
Figure 48: Time-dependent water uptake of the unfilled polymers and the different nanocomposites at a temperature of 30 °C and a humidity of 85%.	58

10.3. List of Schemes

Scheme 1: Functionalization of a silica surface with HMDS. [29]	9
Scheme 2: Crosslinking reaction of an epoxide cured with an amine-based hardener.	11
Scheme 3: Three-step synthesis of 2-but-3'-enyl-2-oxazoline according to Schlaad.	14
Scheme 4: Synthesis of 2-but-3'-enyl-2-oxazoline according to Hoogenboom.	14
Scheme 5: Synthesis of 2-oxazoline monomers according to Witte and Seeliger. ..	15
Scheme 6: Synthesis route of 2-oxazoline monomers according to the Henkel patent.	15
Scheme 7: Cationic ring-opening polymerization of 2-oxazolines with methyl tosylate as initiator.	16
Scheme 8: Mechanism of the thiol-ene click reaction.	17
Scheme 9: Mechanism of the polycondensation of polysiloxanes. [65]	18
Scheme 10: Mechanism of the hydrosilylation of polysiloxanes. [69, 70]	19
Scheme 11: Synthesis of 2-dec-9'-enyl-oxazoline and 2-nonyl-oxazoline according to Henkel-Patent.....	21
Scheme 12: Microwave-assisted synthesis of the copolymer pNonOx ₈₀ -stat- pDec ⁻ Ox ₂₀	23
Scheme 13: Functionalization of the surface of SiO ₂ nanoparticles.....	24
Scheme 14: Covalent embedment of the SiO ₂ -MPTMS nanoparticles in the DGEBA- based polymer matrix.	29
Scheme 13: Covalent Embedment of the SiO ₂ -MPTMS nanoparticles in the polysiloxane-based polymer matrix.	30
Scheme 16: Covalent Embedment of the SiO ₂ -MPTMS nanoparticles in the poly(2- oxazoline)-based polymer matrix.....	31
Scheme 17: Synthesis of 2-dec-9'-enyl-oxazoline according to the Henkel-Patent.	64
Scheme 18: Synthesis of 2-nonyl-oxazoline according to the Henkel-Patent.	65
Scheme 19: Microwave-assisted statistical copolymerization of Dex ⁻ Ox and NonOx.	66
Scheme 20: Surface functionalization of commercially available SiO ₂ nanoparticles.	66

10.4. List of Tables

Table 1: Different kind of polymers and composites used in this investigation.....	21
Table 2: Retention times, the mass-to-charge ratio, and suggested structures of the cleaved off species.	27
Table 3: Glass-transition temperatures of the different polymers and nanocomposites.	32
Table 4: Activation energies for the curing of the different epoxy resins according to Kissinger.....	33
Table 5: Activation energies for the curing of the different polysiloxanes according to Kissinger.....	36
Table 6: Activation energies for the curing of the different poly(2-oxazoline)s according to Kissinger.	38
Table 7: Real and imaginary part of the permittivity of the different epoxy resins at 40 Hz and 20 °C.	49
Table 8: Dielectric Loss of the different epoxy resins at 40 Hz and 20 °C.....	50
Table 9: Real and imaginary part of the permittivity of the different polysiloxanes at 40 Hz and 20 °C.....	51
Table 10: Dielectric loss of the different polysiloxanes at 40 Hz and 20 °C.	52
Table 11: Real and imaginary part of the permittivity of the poly(2-oxazoline)s at 40 Hz and 20 °C.	53
Table 12: Dielectric loss of the different poly(2-oxazoline)s at 40 Hz and 20 °C.....	54
Table 13: Different kind of polymers and composites used for this investigation.	56
Table 14: Dielectric loss of the unfilled polymers and different nanocomposites in dry and wet state (20 °C, 50 Hz).....	59